12-2018

Studying Mechanical and Structural Properties of β-LG and β-CN Fibrils Using Atomic Force Microscopy

Hugo A. Villar
The University of Texas Rio Grande Valley

STUDYING MECHANICAL AND STRUCTURAL PROPERTIES OF β-LG AND β-CN FIBRILS USING ATOMIC FORCE MICROSCOPY

A Thesis

by

HUGO A. VILLAR

Submitted to the Graduate College of
The University of Texas Rio Grande Valley
In partial fulfillment of the requirements for the degree of

MASTER OF SCIENCE

December 2018

Major Subject: Physics

STUDYING MECHANICAL AND STRUCTURAL PROPERTIES OF β-LG AND β-CN FIBRILS USING ATOMIC FORCE MICROSCOPY

A Thesis
by
HUGO A. VILLAR

COMITEE MEMBERS

Dr. Ahmed Touhami
Chair of Committee

Dr. Karen Martirosyan
Committee Member

Dr. Andreas Hanke
Committee Member

December 2018

ABSTRACT

Villar, Hugo A., Studying Mechanical and Structural Properties of β-LG and β-CN Fibrils Using Atomic Force Microscopy. Master of Science (MS), December, 2018, 49 pp., 25 figures, references, 31 titles.

Amyloid fibrils from milk proteins have recently been the subject of extensive investigations in biophysics. The purpose of this thesis is to investigate the dynamics of fibrillation and the mechanical properties of β-LG and β-CN fibers using AFM-Quantitative Nanomechanical Mapping (QNM) and AFM-force spectroscopy. β-LG required one day of heating at 80 ^{o}C , pH 2 to fibrillate in solution; β-CN required three days. Using the AFM-QNM mode an average elastic modulus of 4.3 GPa was determined for the β-LG fibers and 3.1 GPa for β-casein fibers. A persistence length of 920 nm was determined using end to end distance and contour length data of β-LG fibers; for β-casein, a persistence length of 2200 nm was determined.

ACKNOWLEDGMENTS

I want to thank the UTRGV faculty and staff for all their help when I ran into difficulties with the format of the thesis. Special thanks go to the chair of my thesis committee, Dr. Ahmed Touhami, for his patience during the experimental portion of my research and for his guidance and commentary that was of great help for the writing of this thesis. Also give my thanks to the thesis committee members, Dr. Karen Martirosyan and Dr. Andreas Hanke, for providing their input and being part of my academic career.

TABLE OF CONTENTS

LIST OF FIGURES

Page

CHAPTER I

INTRODUCTION

Amyloid fibrils are insoluble self-assembled protein aggregates with a fibrillar shape and a characteristic β-strand rich structure produced from mostly insoluble proteins under certain conditions; these are being found in tissue, body organs and can be formed from various food proteins [1,2]. In recent years amyloid fibrils have become a major subject of study in biophysics and biochemistry due to the role they play in disease and possible applications in medicine, food, and nanotechnology [2]. Networks of amyloid fibrils could be used as scaffold for tissue engineering and to promote neuronal cell attachment and growth [2]. Due to their high resistance to heat (stable up to temperatures of 100 ºC) and enzyme degradation, the fibrils have been proposed as a new method of drug delivery or even to be used as drug themselves [2]. Protein nanofibrils have been successfully used as a template to build metal nanowires and due to their low cost and ease of production the fibrils are considered a promising material for nanoelectronics and light emitting diodes [2]. Besides possible applications, the process of Amyloid fibrillation in itself has been described as belonging to the wider issue of protein folding, which is one of the great unsolved problems in science [3].

1.1. Amyloid Fibrils from Milk Proteins

Many proteins present in bovine and human milk are known to self-assemble into amyloid like fibrils when heated at low pH. Fibrils from bovine milk proteins can form networks with high bulk viscosity and low density, making them attractive and economical for use in medicine and food texturing [4]. The fibrils are considered as a potential new ingredient used for thickening, gelling and for creating low calorie foods and meat replacements [5]. Among the proteins present in bovine milk two have been especially relevant for recent amyloid research: Betalactoglobullin (β-LG) and Caseins; these proteins make up 12% and 80% of all bovine milk protein respectively. β-LG is the main bovine whey protein while caseins are a family of phospholipid proteins known to form fibrils at physiological conditions [5]. The caseins are of four types of polypeptide chain,αs1-CN, αs2-CN, β-CN, and κ-caseins; the different caseins are distinct molecules but are similar in structure. β-LG and κ-casein can coaggregate during heat treatment of milk or after the milk expires. Further research on this phenomenon could improve milk products quality and shelf life as well as help understand age related diseases which involve coaggregation and plaque formation such as Parkinson's and Alzheimer's [6].

1.2. Aggregation of Proteins into Fibrils

During the formation of amyloid fibrils in solution the native conformation of the protein partially unfolds, this promotes aggregation (trough H-bonds, salt bridges, steric interactions) of the partially unfolded protein into an oligomer nucleus with a characteristic tertiary structure (lag phase in Figure 1B); further aggregation occurs at the ends of the nuclei at an accelerated pace (elongation phase in Figure 1B) until protofibrils and fibrils are formed. Fibril formation and growth can be accelerated by adding pre-fabricated nuclei (seeds) into the protein solution, this is known as seeded fibrillation (black curve in Figure 1B) [2,7].

The general mechanism by which amyloid fibrils are formed from a precursor protein can be roughly summarized as occurring in a sequence of steps:

1. Partial denaturation: A change in the environment conditions (pH, heat, agitation, pressure) makes the native state of the protein monomer unstable which promotes partial unfolding and leaves a backbone segment exposed to interactions with other partially unfolded monomers [7,8].

2. Formation of an oligomer nucleus: Partially unfolded monomers bind to each other through hydrophobic interactions and salt bridges and their exposed amide N-H groups and C=O groups forming hydrogen bonds (this binding is not normally possible for native proteins due to repulsive interactions). A few partially unfolded monomers bind to form a nucleus which serves as a template for the formation of the fibril [7].

3. Self-assembly/elongation: After an oligomer nucleus has been formed, some models propose that single unfolded monomers will attach to it one by one at its ends while others argue that the nuclei themselves will linearly self-assemble into protofibrils [8]; a certain number of these protofibrils will twist around each other finalizing the fibril [9].

Amyloid fibrils are produced in the laboratory from a concentrated protein solution by changing the pH of the solution, addition of certain solvents, heating, pressure or a combination of these. In nature, fibrils are found in cells or tissue with abnormally high concentrations of a specific protein [7].

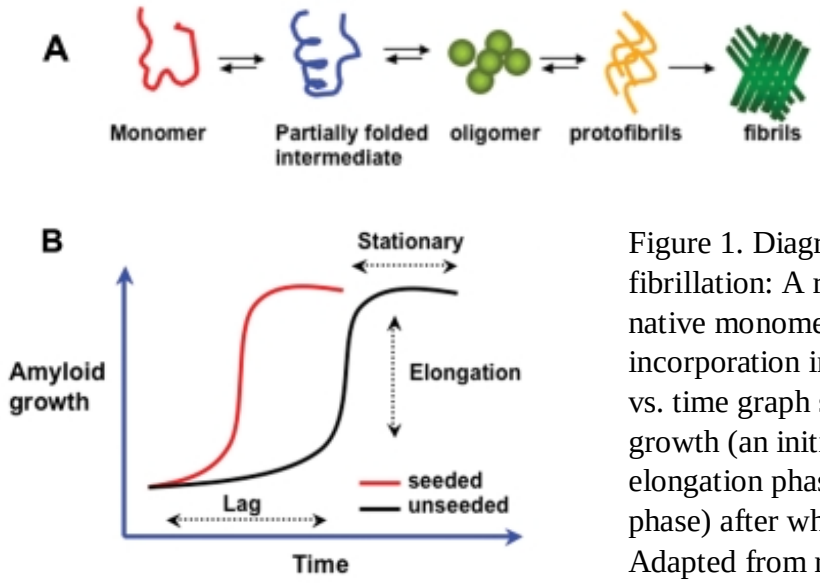

Figure 1. Diagrams illustrating the process of fibrillation: A represents the denaturation of a native monomer and its subsequent incorporation into a fibril; B is a fibril mass vs. time graph showing the phases of fibril growth (an initial lag phase followed by an elongation phase and then reaching a plateau phase) after which no more fibrils form. Adapted from ref. [2].

Several factors are known to influence the fibrillation process and fibril morphology. The initial formation of the nuclei and the aggregation rate are strongly dependent on the concentration of native protein. Because nucleation is a rare stochastic event that requires many unfolded monomers to be within interaction distance of each other, higher concentrations will accelerate the process [7,10]. For some amyloid proteins, a critical concentration has been found below which no noticeable portion of the protein will aggregate into fibrils when subjected to fibrillation inducing conditions [11].

Electrostatic effects play a major role in fibrillation. The elongation/aggregation rate has been found to increase with increased ionic strength and salt concentration, this has been attributed to a decrease in the Debye screening length between the monomers themselves and between monomers and nucleating protofibrils [12,13]. Fibrillation can be accelerated or inhibited by adding polyelectrolytes to prefibrillar solutions; the addition of polyanions was found to accelerate fibrillation of a positively charged proteins while addition of polycations had the opposite effect [13].

1.3. Structure and Mechanical Properties of Amyloid Fibrils

Amyloid fibrils are heterogeneous and unbranching and are made up of individual protofibrils (from 2 to 6 or more) wrapped around each other. It has been suggested most proteins are able to form amyloid fibrils if conditions are appropriate. Fibrils have widths ranging from 6 to tens of nanometers and lengths from 102 nm to 16 μm and those formed from globular proteins have lengths ranging from approximately 50 nm to tens of microns [6]. The persistence length (length over which bending is noticeable, will be explained in more detail next chapter) of amyloid fibrils can vary from few nanometers to several microns.

Proteins from which fibrils are formed come in different sizes and may have very different secondary structures, yet the core structure of all fibrils shares the same basic motif. X ray crystallography revealed that fibrils have a "cross-β" structure, which is a β-sheet conformation in which the hydrogen bonding direction is parallel to the length of the fibril and the β-strands perpendicular, however, the spacing between strands and their direction varies depending on the precursor protein and fibrillation conditions [6]. Some fibrils retain a few non-beta sheet content.

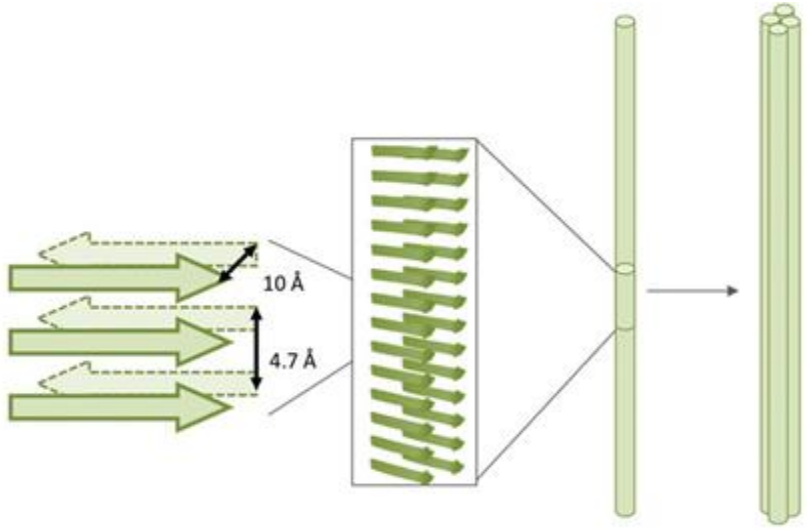

Figure 2. Diagram illustrating the hierarchical structure of amyloid fibrils: The cross-β structural core which linearly self assembles to form proto fibrils, which in turn self-assemble to form mature fibrils. Adapted from ref. [14].

Amyloid fibrils have impressive mechanical properties, especially regarding their modulus of elasticity which generally lies in the Giga Pascal range. The fibrils' mechanical properties can be explained at the molecular level by the presence and density of the hydrogen bonds connecting the beta sheet layers in the fibril. Comparisons between different fibrils reveals a correlation between H-bond density and mechanical strength. Fibrils having protofibril arrangements that maximize the H bond density of the fibril cross section had the highest Young's modulus [15].

Another cause for the fibrils' strength lies in their modular beta sheet structure. When tensile forces are applied on fibrils a successive breaking of the H bonds between beta sheets (much extra energy will be spent breaking these "sacrificial" bonds) will occur until finally the backbone ("hidden length") of the fibril is exposed to elongation and rupture [16]. Additionally, some fibrils' backbones are very extensible and can resist tensile strains of 800% before rupture [17].

1.4. Thesis Objective and Synopsis

The present work consists in the application of two Atomic Force Microscopy (AFM) modes (Peakforce Quantitative Nanomechanical Mapping (QNM) and force spectroscopy) to the study of amyloid fibrils formed from two major proteins present in cow's milk (β-LG and β-Casein) for the purpose of probing their mechanical properties and to better understand their structure and their mechanism of fibrillation.

Chapter II is the materials and methods section. A detailed explanation is given of Atomic Force Microscopy techniques and their application to the study of amyloid fibrils. Background information is given about β-Casein and β-LG proteins and their structure. Sample preparation and software used for data analysis is discussed.

Chapter III presents the results from applying the Peakforce QNM mode to β-LG and β-CN fibrils. Mechanical property data such as Young's Modulus and deformation is presented and discussed as well as information about the geometry and dimensions of the fibrils.

Chapter IV consists on applying the technique of AFM-force spectroscopy on β-LG fibers as well as its native dimer/monomer conformation. The technique is also applied to study β-Casein fibers and monomers as well as its native micelle conformation. From AFM images the structure of the fibrils is analyzed and their persistence length determined.

Chapter V summarizes the results of the previous two chapters and compares these with previous research done on similar proteins. Suggestions are made for future research and possible practical applications.

CHAPTER II

MATERIALS AND METHODS

2.1. β-Lactoglobulin from Bovine Milk

Bovine milk contains 32 grams of protein per liter of whole milk; caseins make up 80% of the milk's protein content with the remaining 20 % made up by whey proteins. The biological role of caseins is to improve digestion in the bovine's stomach and are also a major component in cheese and other foods. Whey proteins are globular proteins and are also used as food ingredients and additives [18].

β-Lactoglobulin (β-LG) makes up more than 50% of all bovine whey protein, it is a globular protein with a radius of gyration of ~ 2.14 nm and it exists mostly as dimers at neutral pH and mostly as monomers at basic or very acidic pH; it contains 152 amino acid residues, which (assuming a length of 0.35 nm per amino acid) yields a length of 58.3 nm for the whole unfolded amino acid chain. The secondary structure of this protein consists mainly of β-strands, some random coil and one α-helix (43.4% β-strand, 6.6% α-helix, 7.1% 3-10 helix and 42.8% random coil); the conformation and shape of the protein does not significantly change or deform when adsorbed onto a surface [19,5]. The full amino acid sequence of the protein is [20]:

LIVTQTMKGLDIQKVAGTWYSLAMAASDISLLDAQSAPLRVYVEELKPTPEGDLEILLQ
KWENDECAQKKIIAEKTKIPAVFKIDALNENKVLVLDTDYKKYLLFCMENSAEPEQSLV
CQCLVRTPEVDDEALEKFDKALKALPMHIRLSFN

2.2. β-Casein from Bovine Milk

β-Casein (β-CN) is one of the four casein types in bovine milk and its human variant is the major casein type present in human milk, making up of 30% of the total milk protein mass [21]; it has an elongated amorphous shape with a gyration radius of ~ 2.73 nm and contains 209 amino acids, yielding a total polymer chain length of ~73 nm [19]. Under ambient conditions and neutral pH, it assembles into micelles, but exists mostly as monomers at very low temperatures and/or concentrations and significantly deforms when adsorbed onto a surface [22,5]; its secondary structure consists mainly of random coil and α-helices [21]. The full amino acid sequence of the protein is [20]:

MKVLILACLVALALARELEELNVPGEIVESLSSSEESITRINKKIEKFQS
EEQQQTEDELQDKIHPFAQTQSLVYPFPGPIPNSLPQNIPPLTQTPVVVP
PFLQPEVMGVSKVKEAMAPKHKEMPFPKYPVEPFTESQSLTLTDVENLHL
PLPLLQSWMHQPHQPLPPTVMFPPQSVLSLSQSKVLPVPQKAVPYPQRDM
PIQAFLLYQEPVLGPVRGPFPIIV

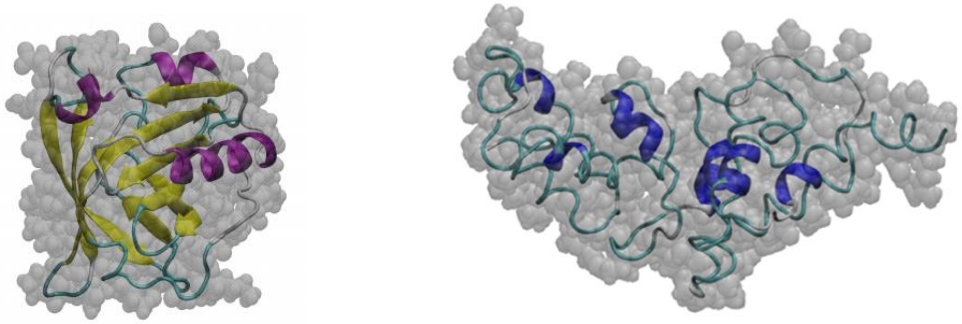

Figure 3. Computer models (obtained from molecular dynamics simulations) of the β-LG (left) and β-CN (right) native monomers showing their secondary structure. β-LG and β-CN are the two main allergic proteins found in cow's milk. Adapted from ref. [19].

2.3. Atomic Force Microscopy (AFM).

Invented in 1986 by Binning et al [23], AFM consists of a nanoscale tip fixed at the end of a cantilever which is brought near to the sample and moved in the x-y plane by a piezoelectric scanner, as the tip scans and interacts with the sample the cantilever bends (deflects) and this deflection is measured by a photodiode which detects the change in direction of a laser reflected of the cantilever's back side (Figure 4A). In the basic imaging mode, contact mode, the measured change in the deflection allows for a topographic image of the sample surface to be obtained. In the other main imaging mode, tapping mode, the cantilever is oscillated vertically near its resonant frequency and then brought near the sample, the interaction of the tip with the sample has an effect on the oscillation amplitude which is detected by the photodiode; from the change in amplitude as the tip scans the surface the topographical image of the sample is obtained [23]. An advantage of AFM when compared with other techniques is that it can be carried out in physiological or liquid conditions (because of this it has proved to be an important tool for the study of amyloid fibrils involved in Alzheimer's and other diseases).

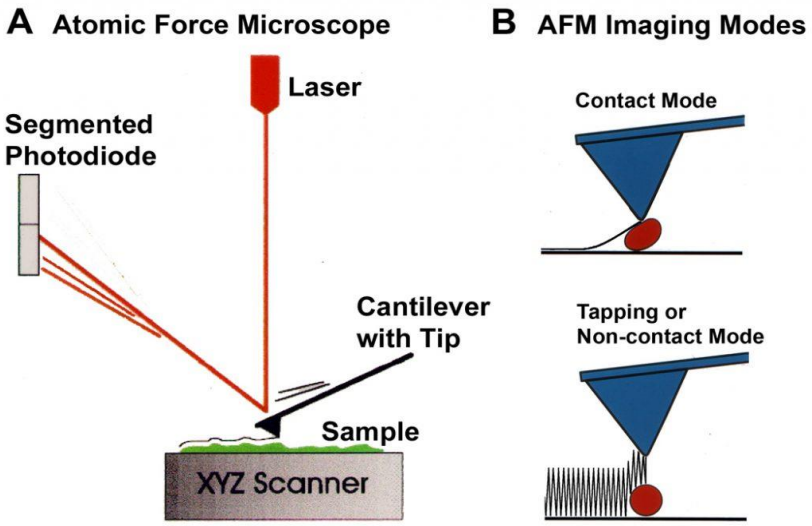

Figure 4. Diagram illustrating the basic setup and principle of Atomic Force Microscopy and its two main imaging modes. Adapted from ref. [24].

2.4. AFM-Quantitative Nanomechanical Mapping (QNM)

The quantitative nanomechanical mapping mode (QNM) allows for the measurement of mechanical properties (Young's modulus, adhesion, deformation and dissipation) at any point in the imaging surface. QNM is a variant of the tapping mode in which the cantilever is oscillated significantly lower than its resonant frequency and force rather amplitude is used as the feedback parameter; The piezo brings the tip close to the sample until a peak force is reached and then retracts the tip back to the starting point to repeat the cycle at a fixed frequency, producing a characteristic heartbeat shaped force vs. time curve for each cycle. The tip interaction with the sample surface is analyzed at each pixel in the image in the form of force vs. separation curves; Numerical models of elastic modulus, dissipation, adhesion, and deformation are automatically fitted to the force curves at each pixel and from this a mapping of the sample's mechanical properties is obtained and superimposed on the topographic image [25].

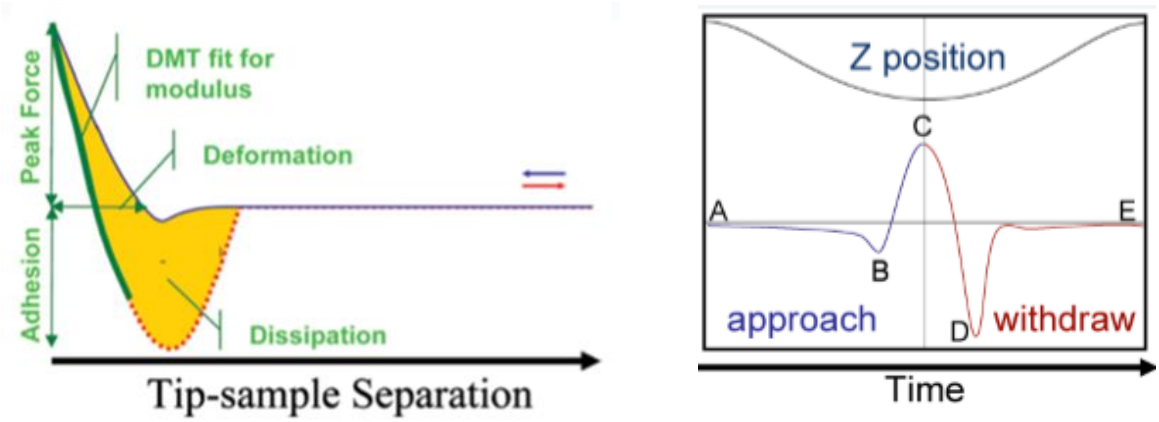

Figure 5. The left image shows a typical force curve used in QNM and the mechanical data that can be extracted from it. On the right is the "heartbeat" force vs. time curve which illustrates the sequence of an approach/retract cycle in QNM and the corresponding piezo height (Z position) superimposed; the peak force at the center of the curve (C) is used as the feedback parameter. Adapted from ref. [25].

2.5. AFM-Force Spectroscopy and Polymer Models

In this mode the tip is moved up and down at a specific location on the sample and by measuring the cantilever deflection (due to the forces of interaction between tip and sample) during this process, a force vs. separation curve is obtained (Fig. 6) [26]. From the force curves important information about the sample can be deduced (such as contour length, persistence length, rupture length, rupture force and secondary structure) by doing statistical analysis and curve fitting using polymer models [27]. Force curves obtained from applying force spectroscopy on proteins have a characteristic sawtooth pattern corresponding to the sequential unfolding of the molecule(s) as it is stretched and the bonds holding the molecule or domains together break down. The sawtooth peaks on the force curves can correspond to the unfolding of subparts of the protein such as β-strands, α-helices, globular domains or entire protein molecules. Because the protein behaves approximately as an elastic polymer chain in between unfolding events, polymer models can be fitted to the peaks in the force curves to obtain information about the contour length released by each unfolding event and the persistence length of the unfolded segment [27].

The simplest polymer model applied to the study of proteins is that of the Freely Jointed Chain (FJC), this model assumes that the polymer chain is composed of straight segments of fixed length and that the orientation of each segment is independent of that of other segments; while sometimes useful, this model is not very accurate when applied to stiffer polymers. The FJC model can be modified into the Freely Rotating Chain (FRC) by setting the angle between successive segments fixed while allowing for free rotation around the axis of the previous segment; taking the continuous limit of the FRC model as the segment length tends to zero and number of segments tends to infinity we arrive at the Worm Like Chain (WLC) model, which is the model used throughout this thesis [28].

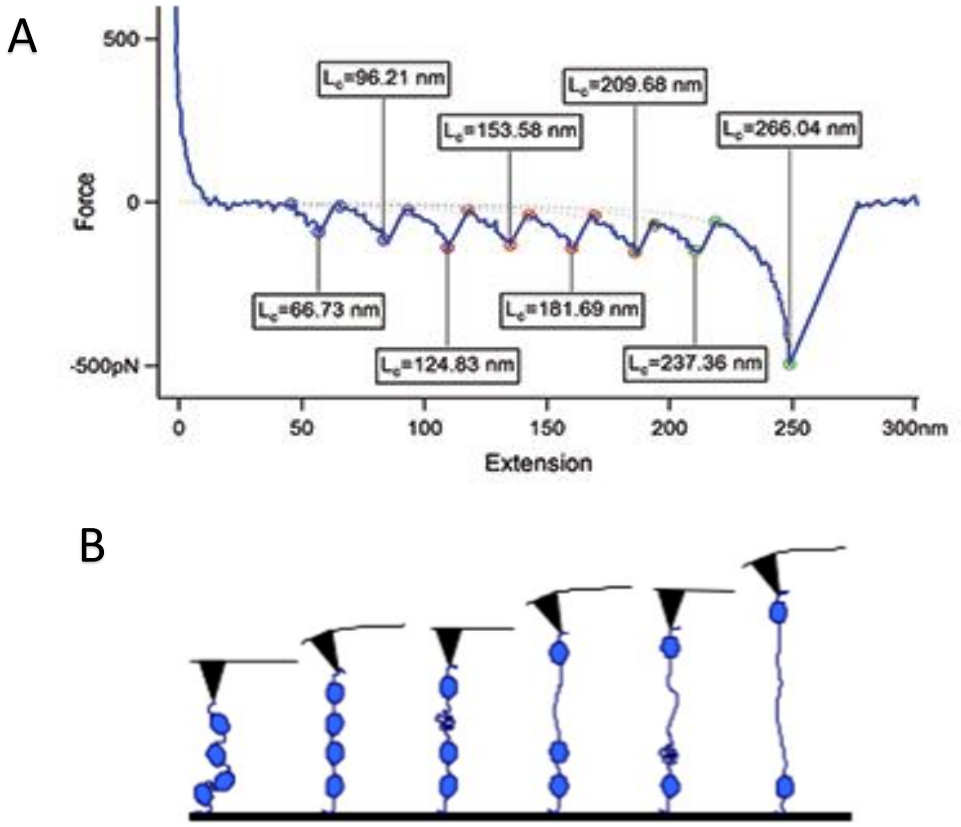

Figure 6. A) shows a typical force curve obtained from doing force spectroscopy on a protein; the curve has a characteristic sawtooth shape, with each peak corresponding to an unfolding event; the peaks are fitted to the WLC model (dotted lines) to deduce the contour length (Lc) released by each unfolding event. B) shows the forced unfolding of a multidomain protein as a sequence, the unfolding of each domain can correspond to a peak on the force curve on A). Adapted from refs. [27,29].

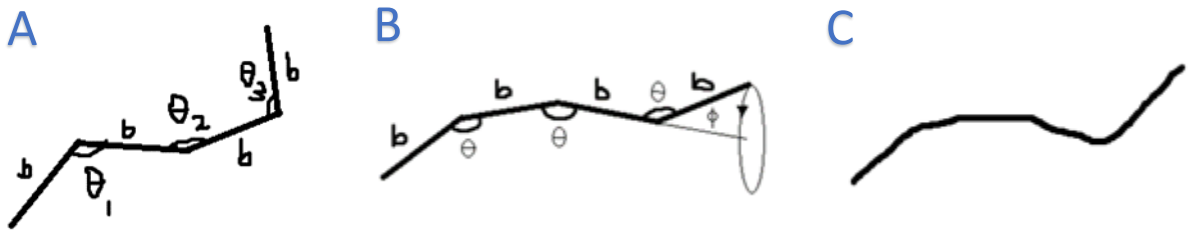

Figure 7. Polymer chain models: A) FJC with fixed segment length b and independent segment orientation. B) FRC with a fixed angle between segments but allowing for free rotation around the previous segment's axis. C) WLC model is the continuous limit to the FRC model (B) as the segment length tends to zero.

A measure of the stiffness of the polymer chain can be deduced by these models by introducing the concept of persistence length Lp (also called the bending length) which is defined as the length over which the angle between successive segments of the polymer chain becomes uncorrelated, or in other words, the length over which the polymer chain direction stops persisting and noticeably bends changing its course [28,30].

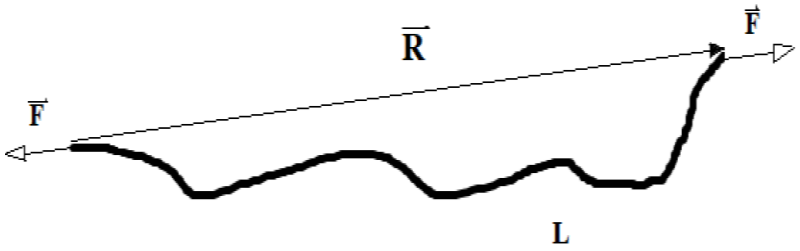

Eq 2.1:

$$\langle R^2 \rangle = \left(\frac{2}{\lambda^2}\right)(\lambda l - 1 + \exp(-\lambda L))$$

Eq 2.2:

$$F = \left(\frac{k_b T}{L_p}\right)\left(\left(\frac{1}{4}\right)\left(1 - \left(\frac{x}{L}\right)\right)^{-2} - \left(\frac{1}{4}\right) + \left(\frac{x}{L}\right)\right)$$

Figure 8. Diagram of a polymer chain in tension and equations for the persistence length Lp and force on a polymer chain as derived from the WLC model: **R** is the end to end vector of the chain, and its magnitude R is the end to end distance, L is the contour length, **F** is the tension force acting at the ends of the chain, x is the extension and λ is equal to 1/Lp. In this thesis eq. 2.1 is fitted to data obtained from AFM images of fibrils and eq. 2.2 is fitted to force vs. separations curves.

With the use of curve fitting software, the WLC model (eq. 2.2) can be fitted to the peaks in force spectroscopy curves; the fitted values of the contour length for successive peaks are then subtracted to deduce the length liberated by each unfolding event; by comparing the unfolded length with reference data the nature of the unfolded length(s) can be determined (whether it corresponds to an unfolded α-helix, β-strand, domain, monomer, etc.) [31]. The WLC model has been applied to AFM-force spectroscopy of amyloid fibrils; the AFM tip may be able to peel off individual β-strands from the fibril [16].

Other information can be extracted from force curves besides contour length or unfolded length. Rupture length is the value of the tip-sample separation at which the sample detaches from the tip, this value can give a hint about the nature of the unfolded protein when a large amount of force curves is obtained for the same sample. Unfolding force is the maximum value of the tip-sample force before an unfolding event occurs, this value corresponds to the peaks of the "sawtooth" on a force spectroscopy curve and can reveal information about the protein's structure and the bonds holding the molecule together.

2.6. Sample Preparation

To produce β-Lg fibrils the following protocol was followed:

1. A 2% wt. solution was made by dissolving powdered bovine β-LG (purchased from Sigma Aldrich) in MiliQ water, the solution was stirred for 30 min with a magnetic stirrer and then centrifuged for 1 hour.
2. pH of the solution was lowered to 2.14 by adding small droplets of HCL and then passed through a 0.45 μm Millipore filter to remove large aggregates or impurities.
3. The filtered solution was heated for 20 hours at 80 ºC on a water heat bath to induce fibrillation; after the heating was completed the solution was quickly cooled down on an ice bath for 30 minutes.
4. The final solution was diluted to 0.2 % wt. to help observe single fibers. A small drop of the solution was adsorbed to freshly cleaved mica surface for AFM measurements.

To produce β-CN fibrils almost the exact same protocol was followed, except a protein concentration of 3% wt. was used and the heating time was increased to 72 hours.

Native β-LG was prepared for imaging by dissolving the powder in MiliQ water (pH 7, standard conditions) at a low concentration (0.2 % wt.) to better observe isolated monomers/dimers on a freshly cleaved mica surface. Initially, native bovine β-CN (also purchased from Sigma Aldrich) was prepared for imaging following the exact same procedure as for native β-LG, but most of the protein observed formed large micelles, therefore, a new protocol was followed to prevent β-CN from forming micelles: A very low concentration solution (0.03% w/v) was made by dissolving powdered bovine β-CN in MiliQ water; The solution was cooled for 30 minutes on an ice bath until reaching a temperature of 5 ºC and then immediately a small drop of solution was adsorbed into the cleaved mica surface for imaging.

2.7. Experimental Setup and Calibration

The AFM model used in this thesis is the Bruker Bioscope Catalyst (Fig. 10) and was controlled using the NanoScope software, all force curves were analyzed using NanoScope Analysis. AFM probes used in this thesis were: Bruker MPP-11100-10 for QNM, with nominal cantilever spring constant of 40 N/m and a nominal tip radius of 8 nm; Bruker MLCT-UMCT-A for force spectroscopy, with nominal spring constant of .07 N/m and nominal tip radius 20 nm.

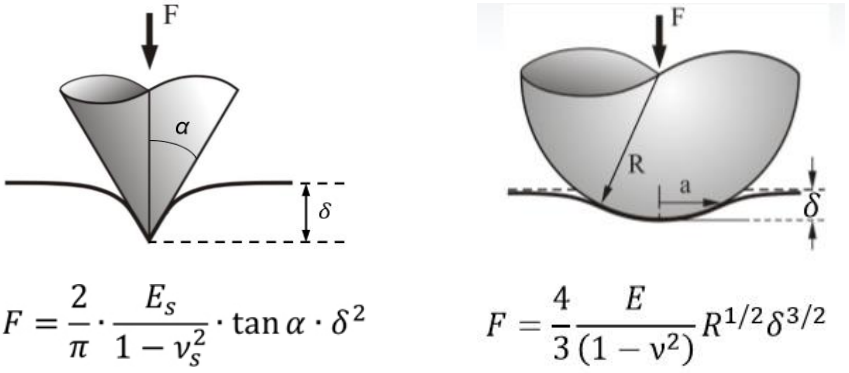

$$F = \frac{2}{\pi} \cdot \frac{E_s}{1-\nu_s^2} \cdot \tan\alpha \cdot \delta^2 \qquad F = \frac{4}{3}\frac{E}{(1-\nu^2)} R^{1/2}\delta^{3/2}$$

Figure 9. Diagram of indentation models used in Peakforce QNM: On the right, the Derjaguin-Muller-Toporov (DMT) model deduces the Young's modulus E of the sample using deformation δ data and tip radius R. On the left is the Sneddon model, where α is the half angle of the indenter (tip). Adapted from ref. [25].

Peakforce QNM (also by Bruker) uses two indentation models (Figure 9) to deduce the Young's modulus of a sample: the Derjaguin-Muller-Toporov (DMT) model which assumes the tip to be spherical in shape and is used for low indentation; and the Sneddon model, which assumes a conical tip and is more suitable for large sample indentations. To implement these models and get accurate results, three parameters must be calibrated first: the deflection sensitivity of the cantilever, the cantilever spring constant and the tip radius.

The procedure followed for Peakforce QNM calibration was:

1. Deflection sensitivity was determined by doing 3 approach/retract (ramp) cycles on a hard (fused Silica) sample so that all deflection was due to cantilever bending with almost no sample deformation; in the 3 corresponding force vs. Z graphs a line fit was done using Nanoscope Analysis on the deflection part of the curve to determine the correct deflection sensitivity.

2. Cantilever spring constant was determined using the thermal tune option on Nanoscope and selecting and fitting the peak corresponding to the cantilever's resonant frequency (written on the cantilever's box).

3. Tip radius was determined by imaging on a Titanium roughness sample (RS-12M from Bruker) and using the Tip Qualification tool on the image in Nanoscope Analysis; then the roughness sample was replaced by a soft sample (PDMS-SOFT-1-12M) and the high speed data capture option was used in Nanoscope to obtain the indentation depth; this value is then inputted back into the tip qualification tool in Nanoscope Analysis to yield the tip radius.

The calibration procedure was repeated many times when QNM results became inaccurate. Only the first two steps were required to calibrate for the force spectroscopy mode.

Other software used throughout this thesis were: ImageJ to measure the contour and end to end length of amyloid fibrils, Excel to produce histograms and charts of the results and Matlab to do some curve fitting.

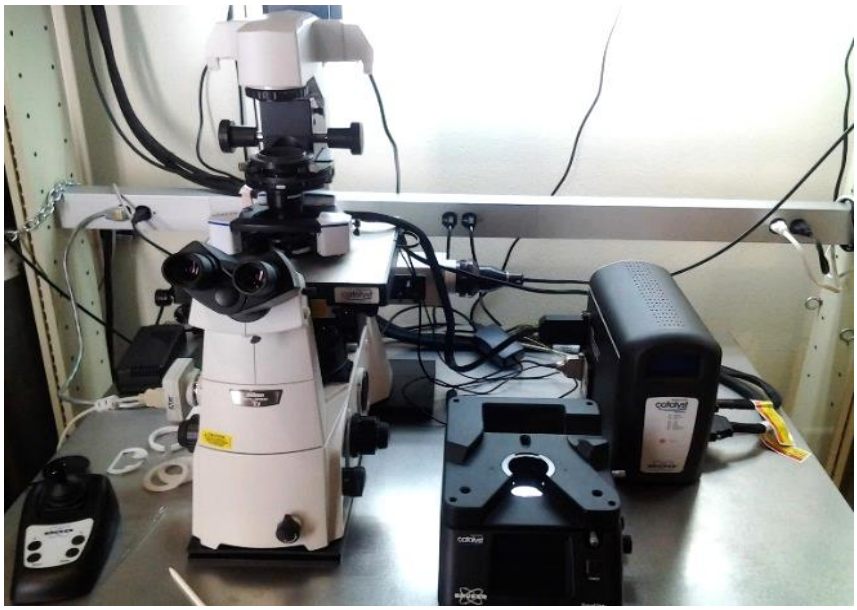

Figure 10. The Bruker Bioscope Catalyst AFM used in this thesis. From left to right: the AFM tip on the piezo stage which raises/lowers the tip with an optical microscope attached to observe the sample from below, the display showing the signal intensity, the Easy Align tool which helps to align the laser with the cantilever and maximize signal, and the computer to control the system.

CHAPTER III

QUANTITATIVE NANOMECHANICAL MAPPING OF β-LG AND β-CN FIBRILS

3.1. Synopsis

As explained in the previous two chapters, all amyloid fibrils have impressive (and similar) mechanical properties due to their sharing the same cross-β tertiary structure; however, the spacing of the β-strands in the fibril and their direction and length can vary depending on the precursor protein. In order to understand in more detail the dependence of the fibril's mechanical properties on its structure (and on its precursor protein) it is necessary to determine the Young's modulus of the fibril using the newest and most precise techniques available.

This chapter will present and discuss the results of applying the technique of AFM Peakforce QNM to study the mechanical properties of β-CN and β-LG amyloid fibrils, some of the structural properties (cross sectional profile, height and shape) of the fibrils and also the effect of heating time and protein concentration on the process of fibrillation. The results for the fibrillation process are presented as a sequence of AFM images beginning with the native protein and culminating with mature amyloid fibrils. Results for QNM measurements are presented using histograms. Some sample QNM images are displayed after the results.

3.2. Results: Fibrillation process

As shown in Figure 11A, at neutral conditions the β-CN protein arranges itself in spherical micelles with sizes between 10 to 20 nm (inset image A). After one day of heating at 80 ^{o}C the micellar structure started to open and form short fibers (image B Figure 11). In addition, many micelles were still visible with the same sizes at the neutral structure. After two days of heating at the same temperature large fibrillar structures started to be visible with maximum diameter around 10 nm. Importantly, at these conditions no large micelles are seen (Figure 11C). Finally, after three days of heating at the same temperature, complete protein fibrils are formed with diameter around 20 nm (Figure 11D). As shown at the bottom part of image D, the fibers are arranged in helical structure.

At neutral conditions (Figure 12A) the β-LG protein exists as a mixture of monomers and dimers with sizes between 2 and 4 nm (inset image A). After two hours of heating at 80 ^{o}C, large aggregates, with sizes around 10 nm, started to form (Figure 12B). After 12 hours of heating at the same conditions, the aggregates started to connect making short fibrillar structures (Figure 12C). Finally, after twenty hours of heating at the same temperature and conditions, fully formed fibers were observed (Figure 12D). As shown in the inset of image D the AFM cross-section profile indicates that the diameters of the fibers are between 2 and 4 nm which are the sizes of the proteins at the native conditions.

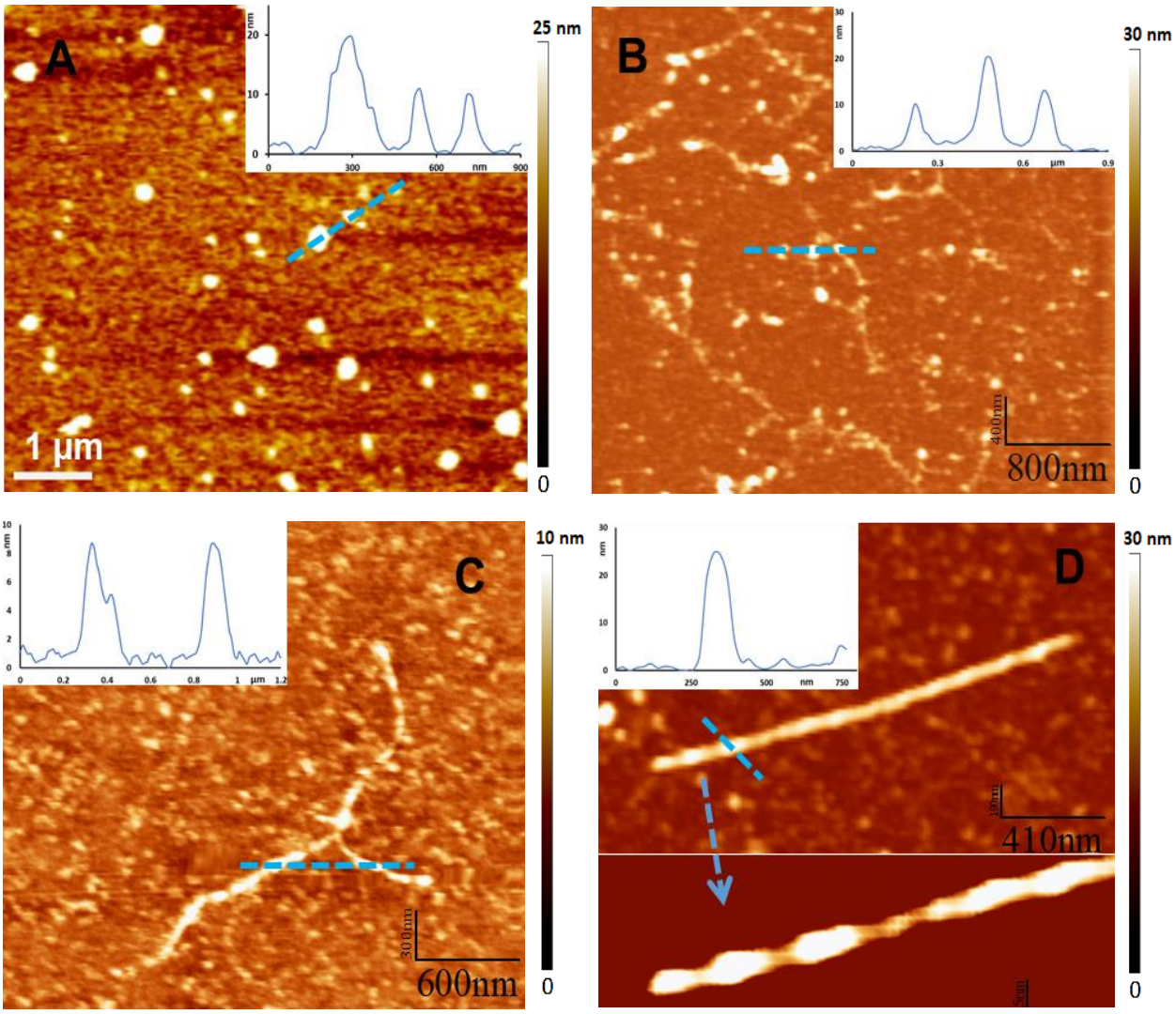

Figure 11. AFM images showing the effect of the heating time (80 °C at pH 2 and 3% w/v) on the fibrillation of β-CN. (A) the protein in its native micelle form at pH 7 before heating.(B) after 1 day of heating proteins start to connect to each other. (C) after 2 days of heating some fibrils can be imaged. (D) after 3 days of heating fully formed fibrils were observed. (insets are AFM cross-section showing the size of the imaged structures).

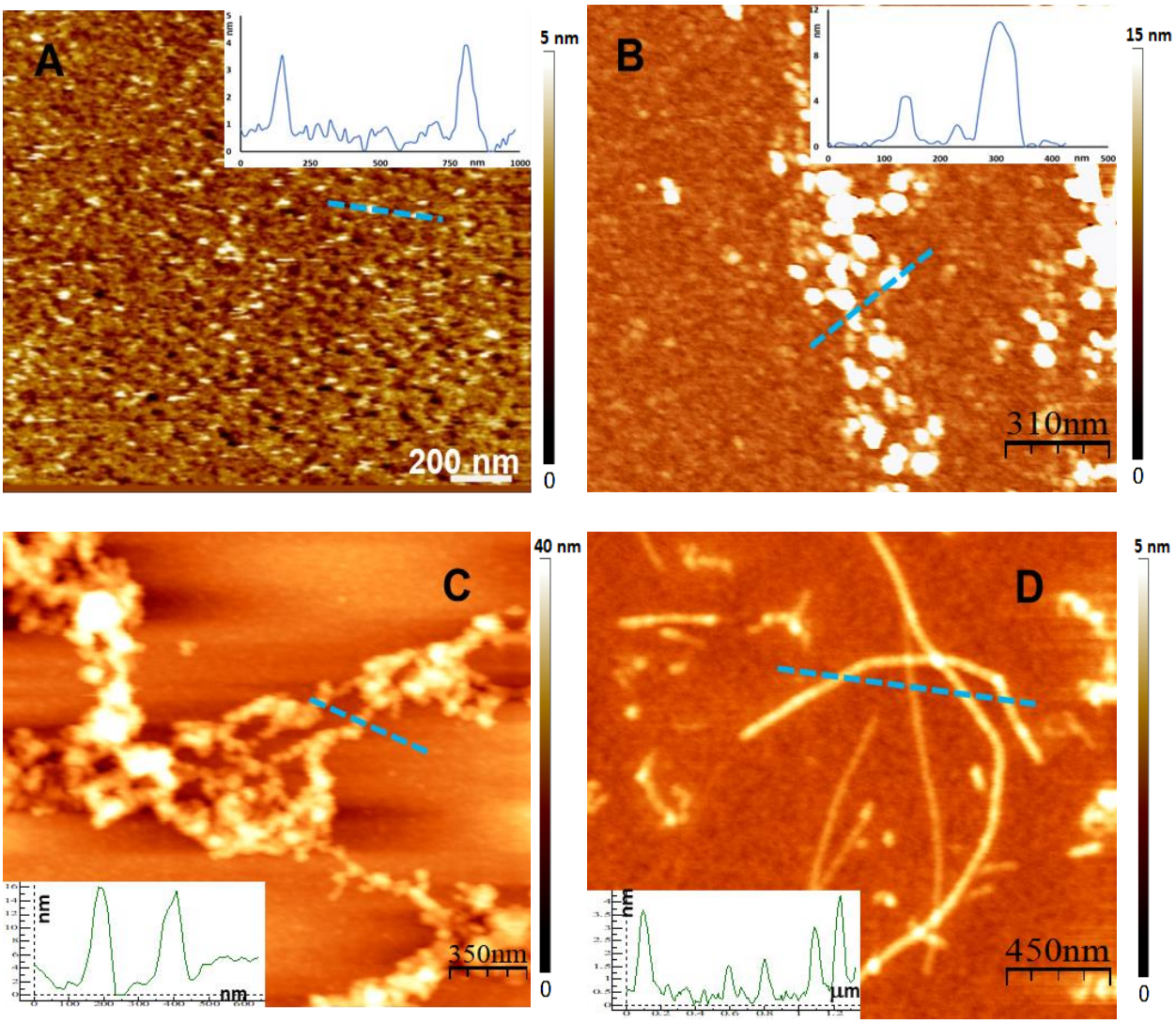

Figure 12. AFM images of the effects of heating time and concentration on the fibrillation of β-LG at pH 2. (A) the protein in its native dimer/monomer form at neutral pH and 0.2% wt. (B) after 2 hrs. of heating at 80º C (0.2 % wt.) proteins start to aggregate. (C) after 6 hrs. of heating at 80º C (0.2 % wt.). short fibrillar structures can be imaged. (D) after 20 hrs. of heating at 80º C (2 % wt.). fully formed fibrils were observed. (insets are AFM cross-section showing the size of the imaged structures).

3.3. Results: Mechanical Properties and Structure

As can be seen from the height measurements histogram (Figure 13A) β-CN fibrils were much thicker on average than β-LG fibrils (Figure 13B) but also had a much wider variety of heights (from approximately 10 nm to 35 nm) than β-LG fibrils (from approx. 1 nm to 7 nm). An average value of the Young's modulus of 4.3 GPa was obtained for β-LG fibrils (Figure 14A) and 3.1 GPa for β-CN fibrils (Figure 14B). β-CN fibrils were overall more deformable than β-lg fibrils (Figure 14D), in agreement with their lower Young's modulus when compared to β-lg fibrils. Figure 15 and Figure 16 display some sample QNM images of β-CN and β-LG fibrils and show the bumped profile some fibrils have when looking at their cross section along the fibril's length (Figure 15E, Figure 16E). In Figure 15B, β-CN fibrils are seen either being formed from protofibrils or being disentangled into their component protofibrils.

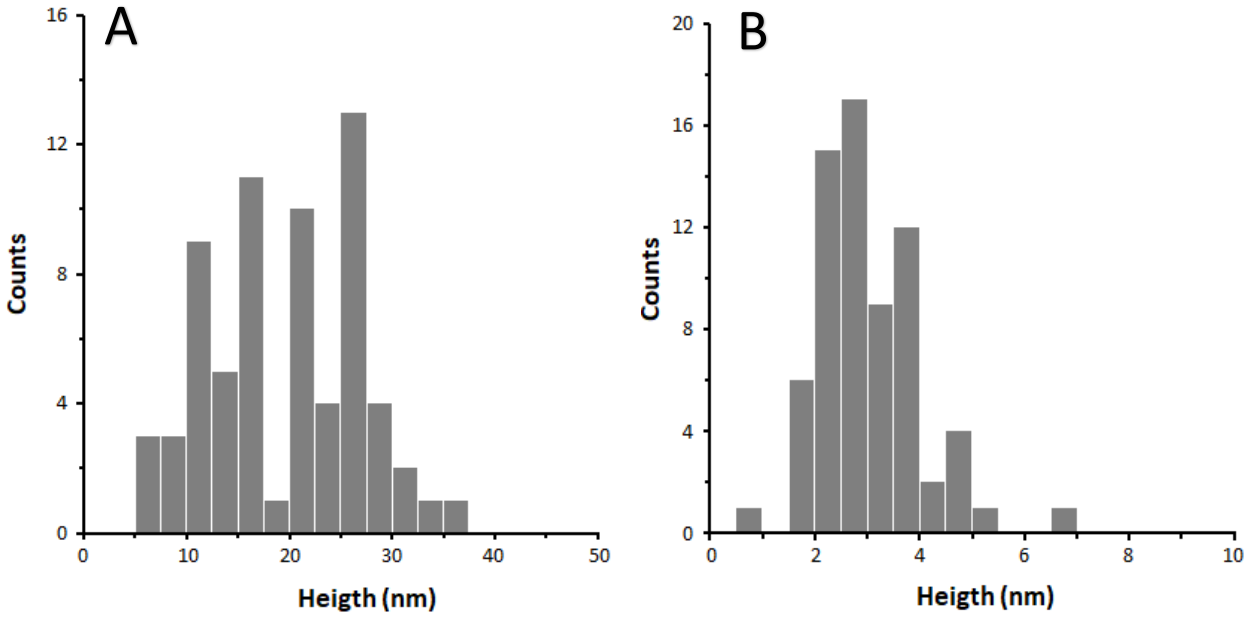

Figure 13. Histograms of fibril height data obtained from AFM height images: (A) height data for β-LG fibrils; (B) height data for β-CN fibrils.

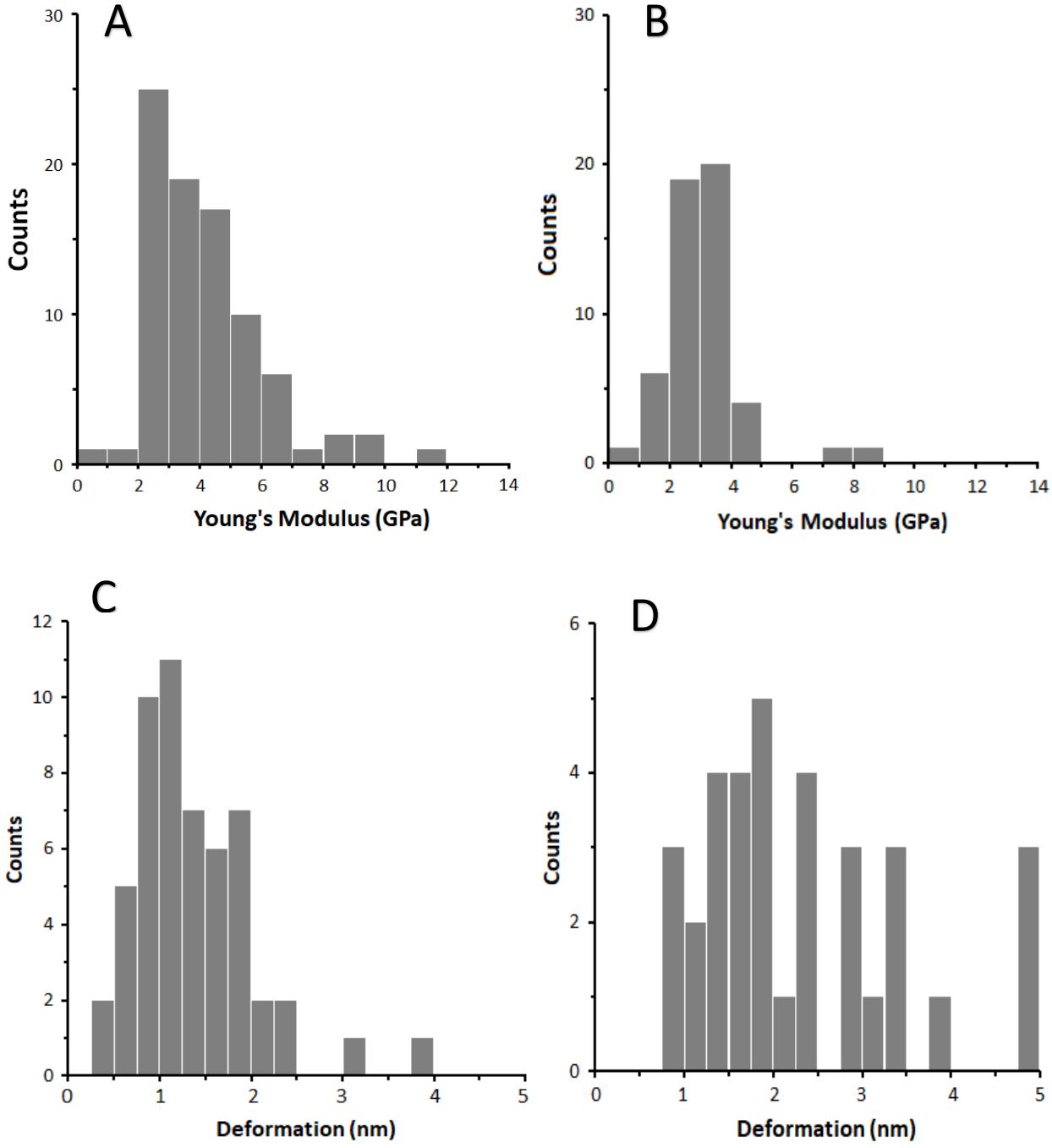

Figure 14. Histograms of Young's modulus and deformation data of β-LG and β-CN fibrils, obtained from Peakforce QNM measurements. (A) Young's modulus data for β-LG fibrils; (B) Young's modulus data for β-CN fibrils; (C) deformation data for β-LG fibrils; (D) deformation data for β-CN fibrils.

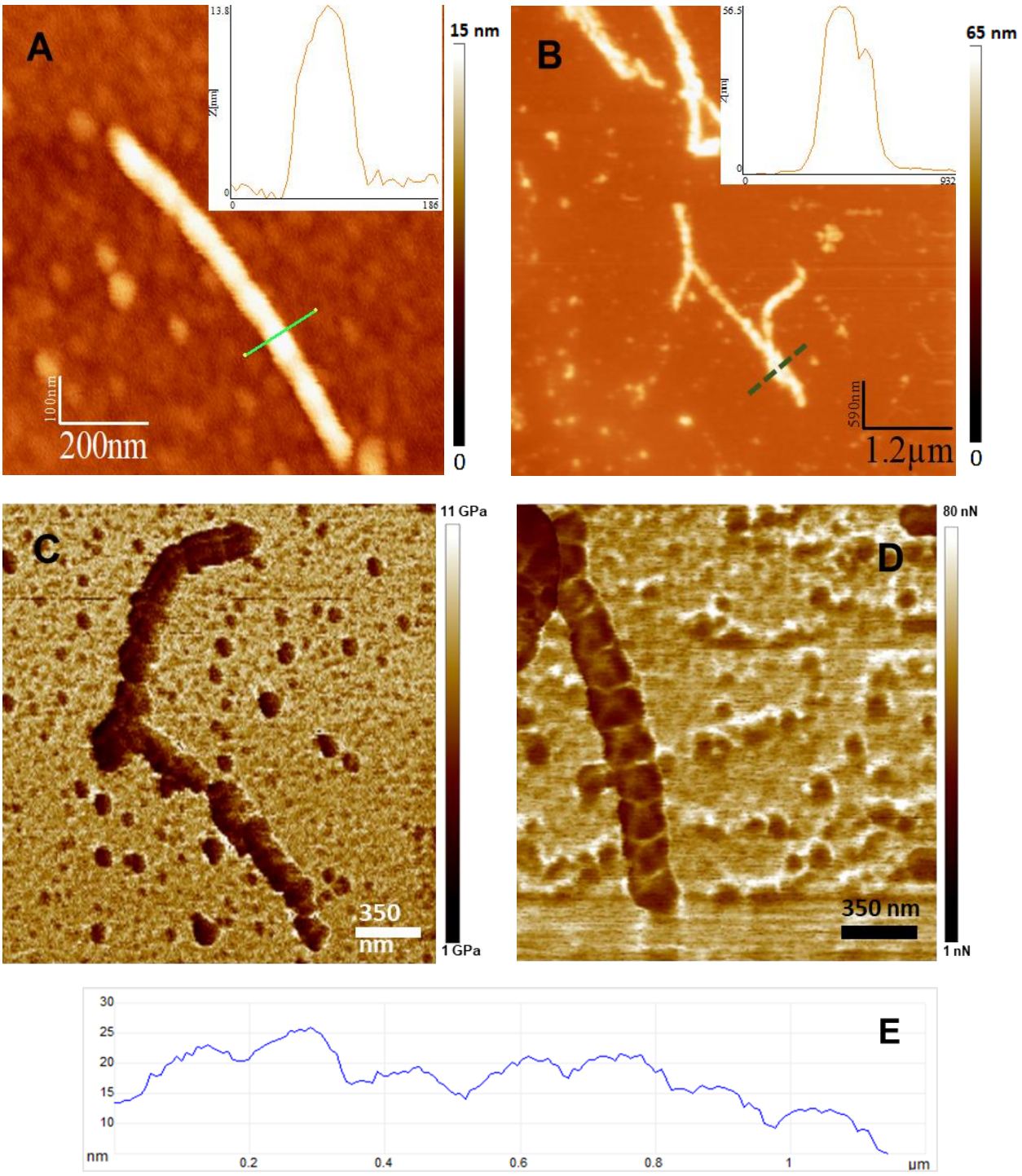

Figure 15. Peak Force QNM images of β-casein fibrils: (A) height image of a fibril; (B) protofibrils coalescing to a mature fibril; (C) modulus image; (D) adhesion image showing the segmental bumped shape of some fibrils; (E) cross sectional height profile along the length of the fibril from (D) showing a height periodicity of ~150 nm.

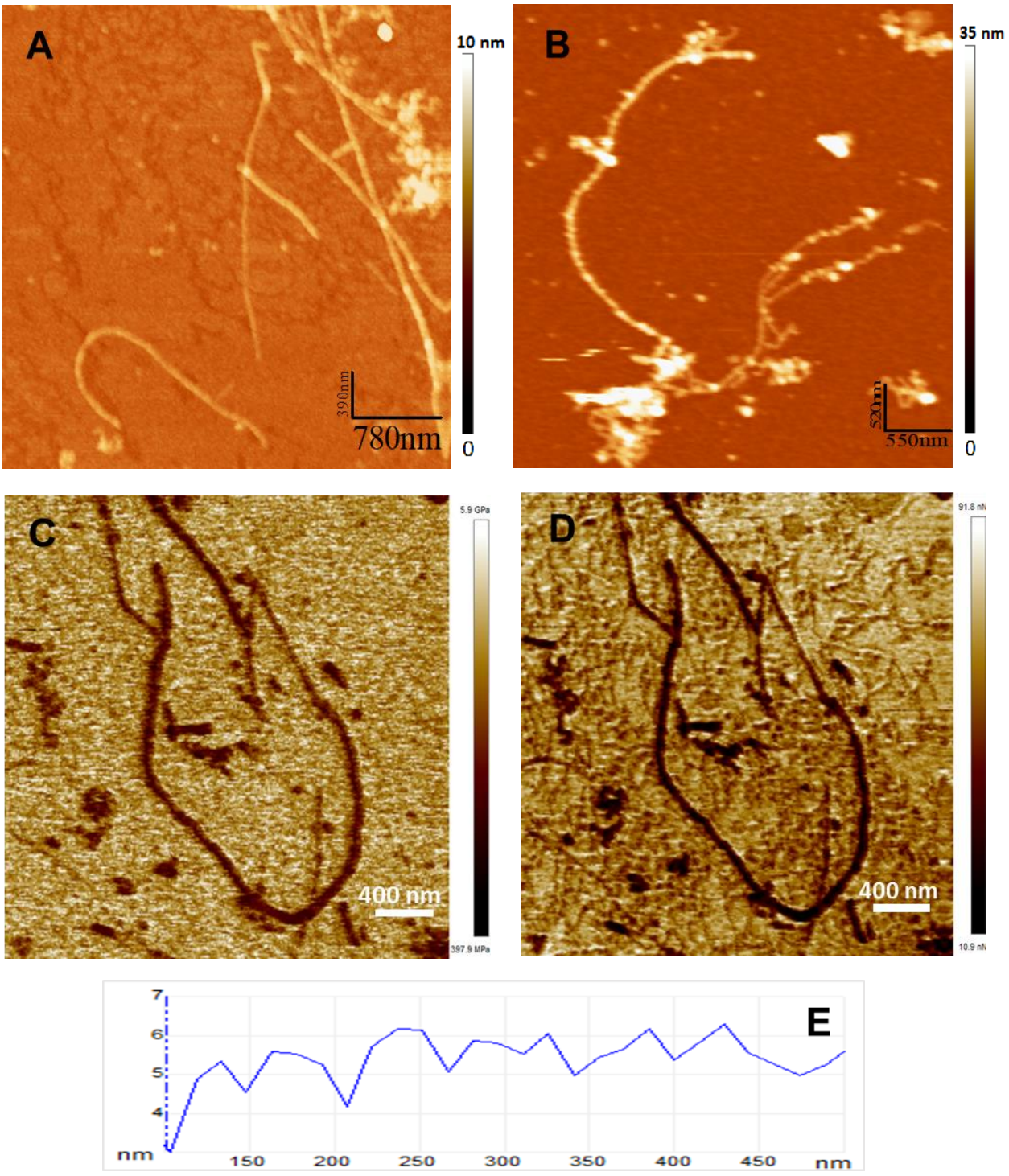

Figure 16. Peak Force QNM images of β-LG fibrils: (A) height image; (B) height image showing thin protofibrils being incorporated into a thicker mature fibril; (C) modulus image; (D) adhesion image; (E) cross sectional height profile along the length of a β-LG fibril showing a height periodicity of ~50 nm, much lower than that of β-CN fibrils.

3.4. Discussion

The process of producing the fibrils was the initial and most difficult step for the investigation (several attempts had to be made throughout many weeks), however, it yielded the most interesting results. For β-LG fibrillation was very straightforward (after determining the right protein concentration of 2% w.t) requiring 20 hours of heating at 80 ^{o}C for fully formed fibrils to be visualized by AFM. Although there were still a lot of amorphous aggregates remaining, the concentration required to see fully formed β-LG fibrils closely agrees with previous studies (2.5 % w.t was the critical concentration for our reference). For β-CN, fibrillation required three full days of heating at 80 ^{o}C, after which mature fibrils (a few linear aggregates were seen after two days) were observed along with disordered aggregates and protofibrils (Figure 11) which were on the process of forming mature fibrils. This result does not agree with our reference protocol which only required one day of heating at 90 ^{o}C. Because previous studies on casein amyloid fibrillation have focused mostly on the other caseins (we could only find one clear reference protocol for the fibrillation of β-casein) this opens the possibility that there is a threshold temperature (higher than 80 ^{o}C) beyond which β-CN fibrillation is accelerated.

One factor that could explain the difference in the heating time required for the fibrillation of the two proteins is their drastically different native structures. The native β-LG contains a high amount of β-strand content when compared to β-CN, which according to literature, has zero native β-strand content. We speculate that native proteins with higher native β-strand content would require less denaturation and therefore less heat to form a cross-β nucleus and then undergo self-assembly/fibrillation.

The QNM measurements on β-CN and β-LG fibrils, led to the determination of the average Young's modulus of both fibrillary structures (Figure 13). The values found (for β-LG fibrils 4.3 GPa and for β-CN fibrils 3.1 GPa) were close to each other and on the same range as other amyloid fibrils. This is most likely due to the fibrils sharing a common modular cross-β structure as was discussed in more detail on the introduction chapter. Again, the drastic difference in the native structure of the two proteins, makes the similarities of the fibrillar mechanical properties even more striking and highlights the need to study the fibrillation process of amyloids in greater detail.

β-CN fibrils observed were more than twice as thick as β-LG fibrils but also shorter on average than β-LG fibrils (Figure 14). Some of this data will be used on the next chapter to derive the persistence length, from which the Young's modulus can be estimated and compared with the QNM results. The thinnest β-LG fibrils had a height of ~2 nm, half the size of native β-LG monomers, so that these could be individual protofibrils made of unfolded monomers; if this is the case then the thickest fibrils observed are composed of 2 protofibrils. β-CN fibrils had minimum heights of less than 5 nm, but because β-CN monomers are very deformable and not globular it is difficult to tell if isolated protofibrils were observed or if these are made of unfolded monomers. Protofibrils of β-CN were found to bundle together to form a mature fibril (Figure 15B). Some fibrils had a regular bumped worm-like height profile (Figures 15D and 16D), with an average height periodicity of ~ 40 nm for β-LG fibrils and ~ 150 nm for β-CN fibrils. The bumps were most likely due to the arrangement of the component protofibrils in which the protofibrils wrap around each other helically (Figure 11D); fibrils with a flat profile with bumps would be those in which the protofibrils arrange themselves parallel to each other (Figure 2).

Our nanomechanical measurements demonstrated that the Peak Force QNM mode is a powerful tool to investigate the mechanics of amyloid fibrils. Also, our data can serve as an independent verification of the factors which affect the process of amyloid fibrillation such as native protein concentration, pH and heating time. The results obtained allowed for some hypotheses to be made regarding the origin of the mechanical properties of amyloid fibrils and their relation to the native structure of the protein, however, much further research is required to give any validation to these ideas.

Recommendations for future research would include observing in more detail the process of fibrillation, using much higher temperatures up to 100 ^{o}C to test their effect on fibrillation time and to apply the QNM mode at regular time intervals during the fibrillation process to detect changes in mechanical properties as the native protein forms fibrils. Many different proteins with very different native structures should be subjected to similar conditions to induce fibril formation to check whether there is a relationship between the amount of β-strand content in the native protein and the heating time required for mature fibrils to form.

CHAPTER IV

AFM-FORCE SPECTROSCOPY OF β-LG AND β-CN FIBRILS

4.1. Synopsis

AFM images of dozens of single isolated fibrils were analyzed and their contour length and end-to-end distance measured; to determine the fibril's persistence length the data was plotted and least squares fitted in Excel using equation 2.1. Hundreds of force vs. separation curves were obtained by pulling at the surface of dozens of fibrils and also from pulling at the native conformation of the protein. From these force curves data such as rupture length, maximum adhesion, unfolding force, step length was extracted and a statistical analysis was done with histograms.

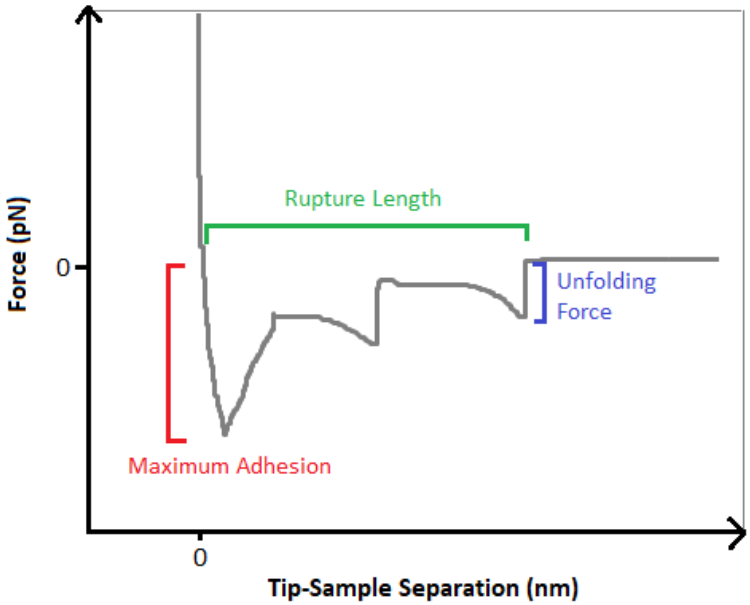

Figure 17. Sample force vs. separation curve illustrating some of the parameters that are extracted and analyzed throughout this chapter.

4.2. Overview of Results

After obtaining the height images of isolated fibrils, the contour length and end to end distance of dozens of fibrils was measured with ImageJ and plotted in a histogram (Figure 18), yielding an average contour length of 1.84 μm for β-LG fibrils and 2.22 μm for β-CN fibrils and an average end to end distance of 1.36 μm for β-LG and 1.93 μm for β-CN. Only single isolated fibrils were taken into account, not those entangled or on top of other fibrils, otherwise β-LG fibrils were overall longer than β-CN ones. The contour length/end to end distance data was plotted and inputted into Excel to do a least squares fit (using eq. 2.1) to obtain an approximate value of the persistence length Lp (Figure 19); the least squares fit yielded a value of 920 nm for the Lp of β-LG fibrils and 2240 nm for β-CN fibrils. These values of the persistence length were then inputted into the correlation function $e^{-x/Lp}$ and the results were plotted in Figure 20.

The analysis of hundreds of force spectroscopy force curves yielded an average rupture length of 114.7 nm for β-LG fibrils, the corresponding rupture length histogram (Figure 23B) had a major peak at ~ 60 nm and a slightly lower peak at ~110 nm. For β-CN fibrils an average rupture length of 49.3 nm was obtained and the corresponding histogram contained a peak at ~ 30 nm (Figure 23). The rupture length histogram for native β-LG had a high narrow peak at ~ 115 nm (Figure 23A), which is close to the unfolded length of a β-LG dimer (106 nm), while the histogram for native β-CN had a major peak at ~100 nm, which is higher than the unfolded length of a β-CN monomer (74 nm). As shown in Figure 24, force spectroscopy of β-CN fibrils yielded similar values for the unfolding force as native β-CN, while β-LG fibrils had unfolding forces much higher than that of native β-LG and almost twice as high as that of β-CN fibrils. Histograms of maximum adhesion (Fig. 25) show β-LG fibrils have much higher adhesion than native β-LG, while adhesion values for β-CN fibrils were similar to that of native β-CN.

4.3. Results: Image Analysis

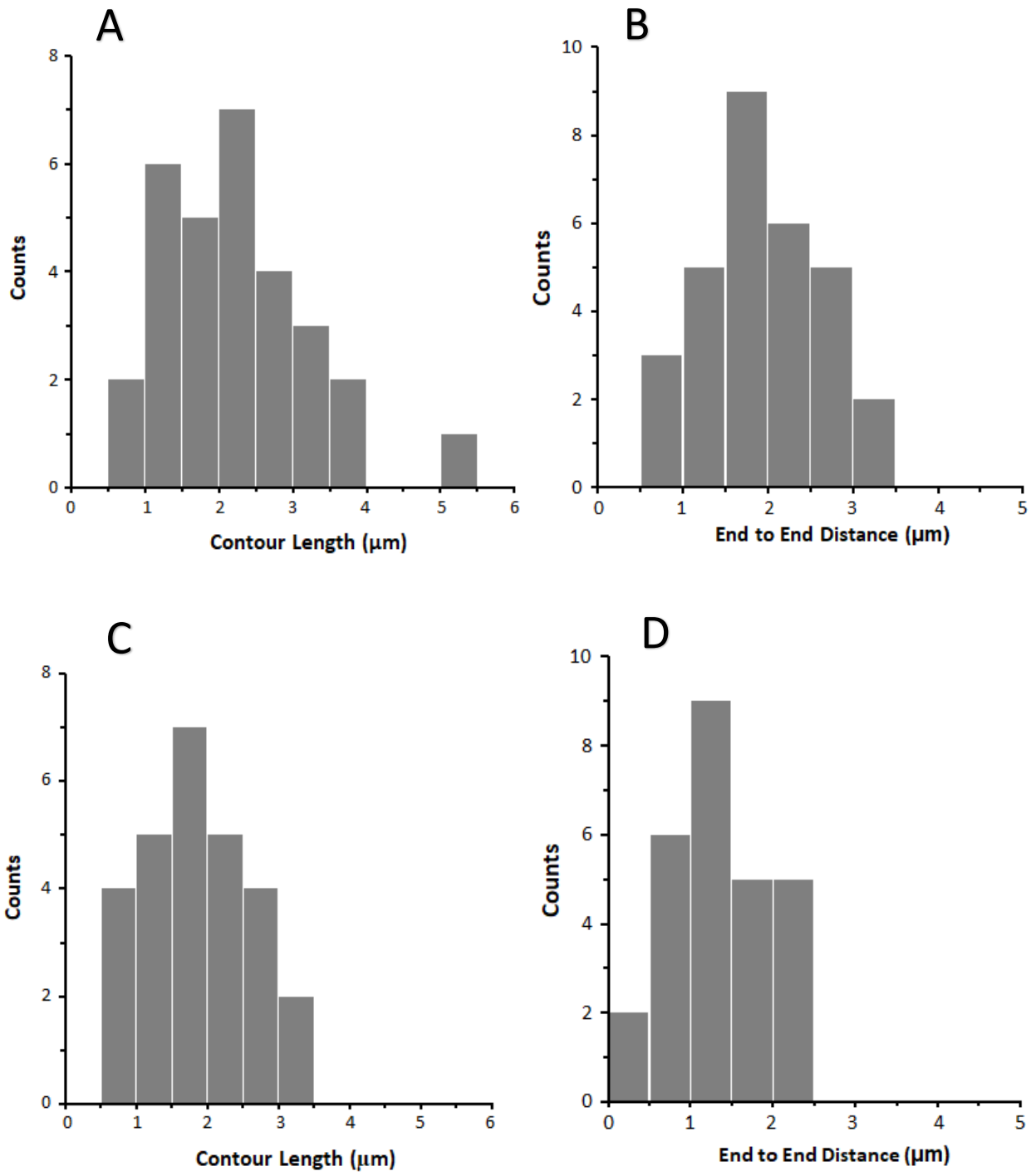

Figure 18. Histograms of contour length and end to end distance for β-CN fibrils (A and B) and β-LG fibrils (C and D) obtained from AFM images. Only single isolated fibrils were part of the analysis, not those that were entangled or on top of other fibrils, otherwise β-LG fibers would have a higher contour length than β-CN fibrils.

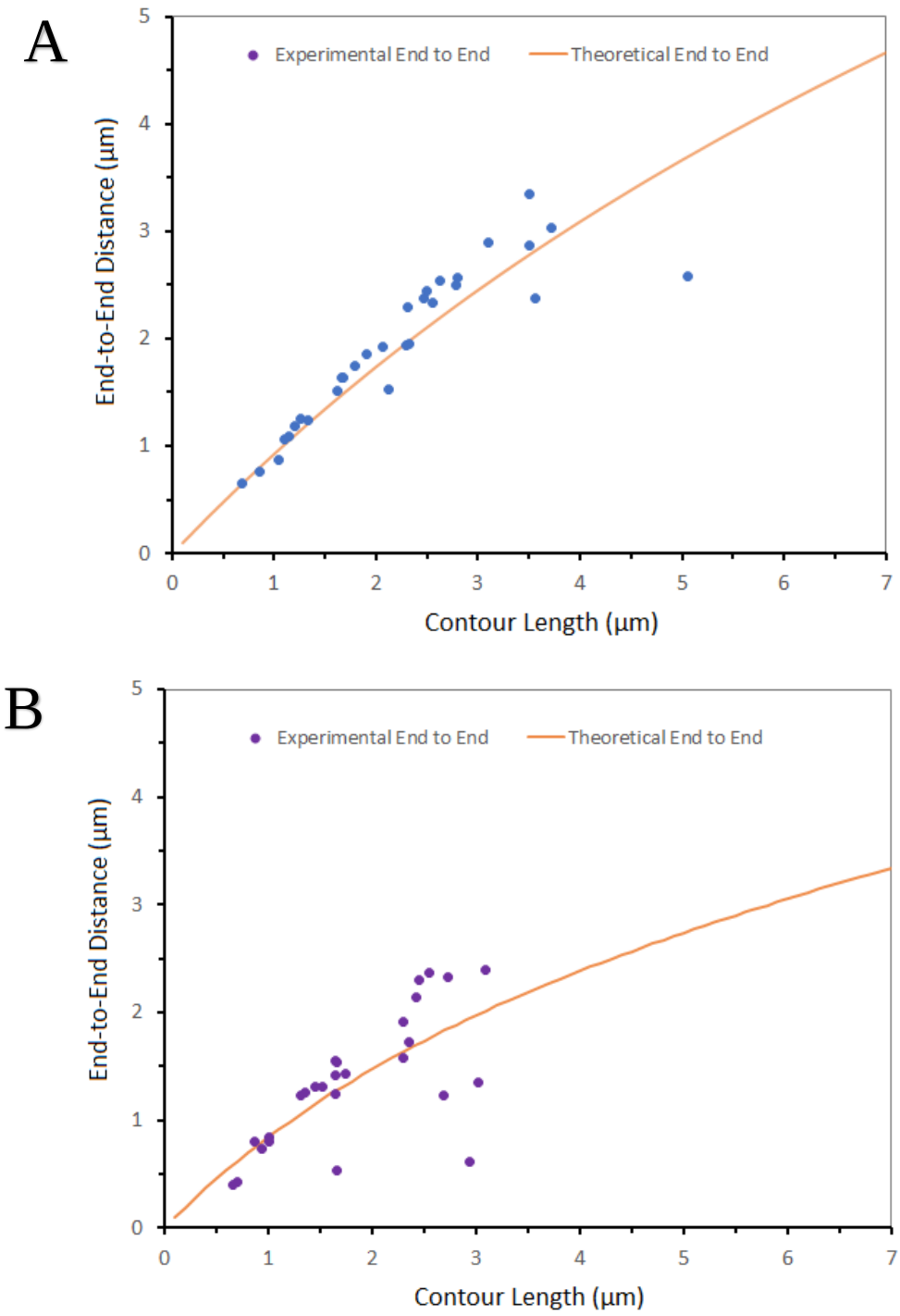

Figure 19. Plots of end to end distance vs. contour length from image data of single isolated fibrils and the theoretical fit using eq. 2.1 with Lp being the fitting parameter. (A) image data for 31 β-CN fibrils yielding a persistence length of **2240 nm**; (B) image data for 29 β-LG fibrils yielding a persistence length of **920 nm**, less than half of that of β-CN fibrils, although this makes sense due to β-CN fibrils being much thicker than β-LG fibrils.

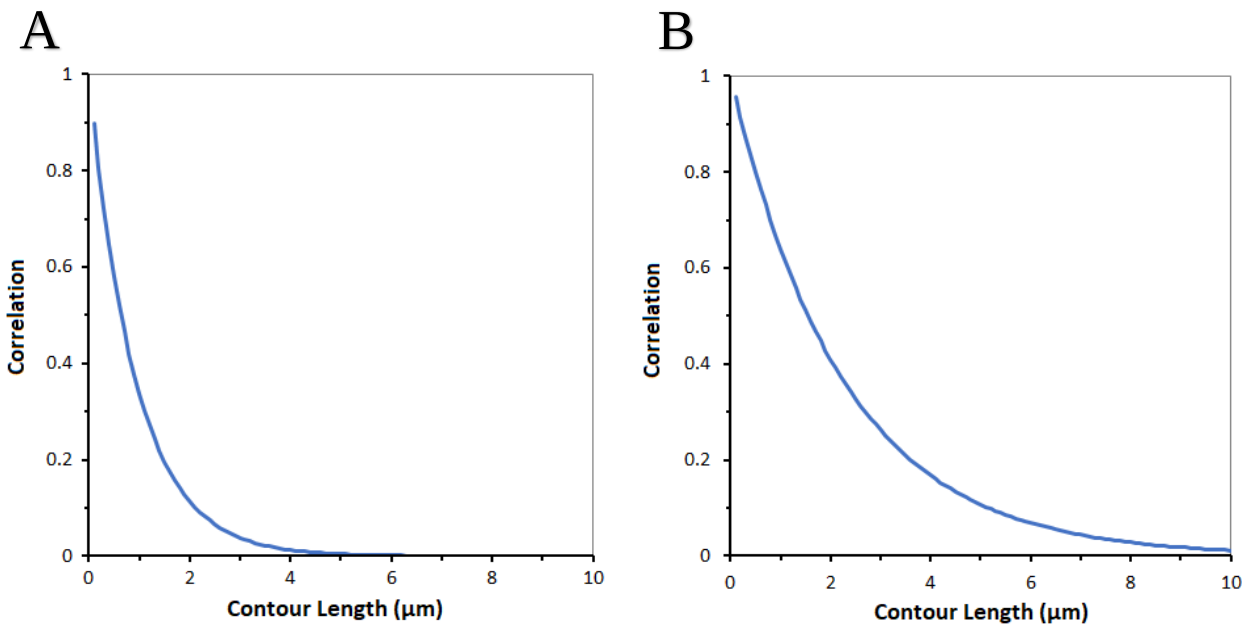

Figure 20. Plots of correlation vs. contour length for (A) β-CN fibrils and (B) β-LG fibrils assuming a WLC model. The correlation function is $e^{-x/Lp}$ where x is the contour length and Lp is the persistence length as derived from the theoretical fit in figure 19.

4.4. Results: Force Curve Analysis

Some sample force spectroscopy force curves for β-LG are shown on the next two pages (Figure 21); all the curves have the characteristic sawtooth shape which allows for doing curve fitting using the WLC model, the model is fitted to the last peak in the force curve to determine the total contour length of the unfolded molecule. Native β-LG force curves, Figure 21A and Figure 21B, yielded an unfolded contour length value close to that of a monomer and a dimer, respectively. The force curve from fibrillar β-LG (Figure 21C) also yielded a contour length value close to that of a β-LG monomer. Figure 22 shows two curves for β-CN; native β-CN forms micelles composed of several monomers (Figure 22A) which explains the high adhesion on the corresponding force curve (Figure 22B), for this force curve the WLC model yielded a contour length close to that of a β-CN monomer.

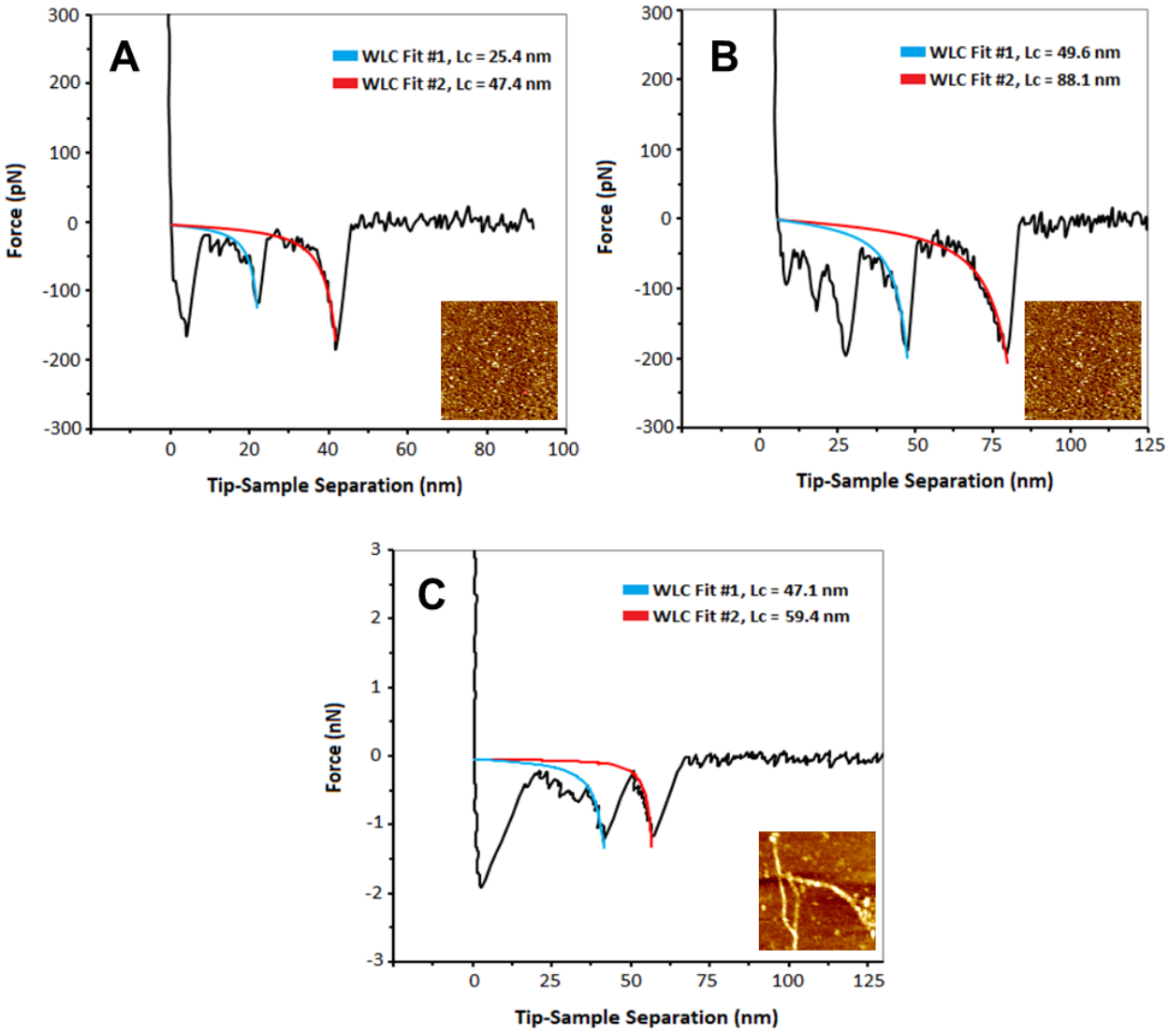

Figure 21. Force spectroscopy of β-LG and curve fitting using the WLC model; the inserted images show the area on the sample in which force spectroscopy was performed: (A) Force curve representing the unfolding of a native β-LG monomer; (B) Force curve most likely representing the unfolding of a dimer; (C) Force curve possibly representing the unfolding of fibril nuclei at the surface of the fibril.

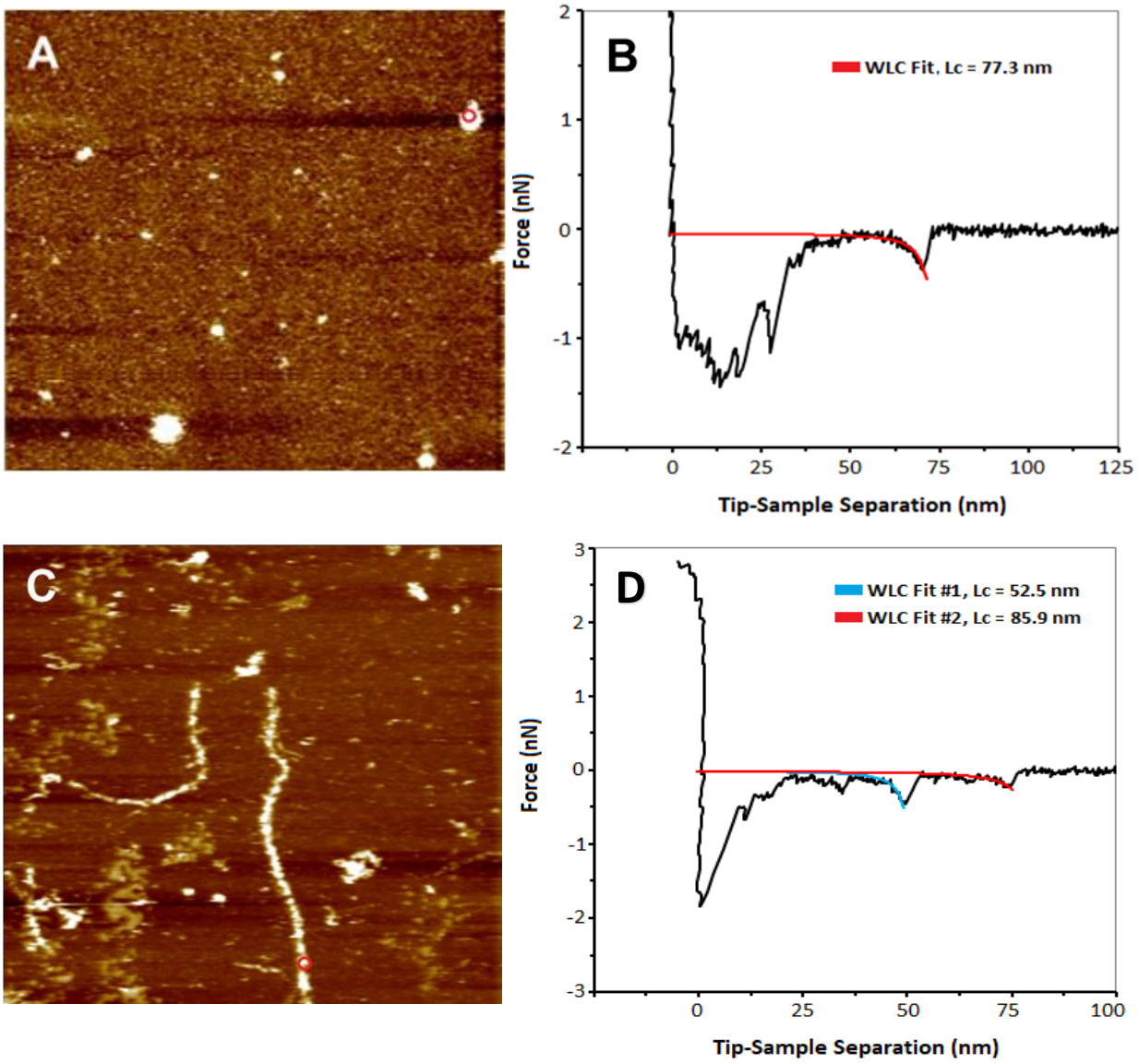

Figure 22. Force spectroscopy of β-CN and curve fitting using the WLC model: (A) 6.2 x 6.2 μm height image of native micellar β-CN ; the red circle indicates the point at which force pulling was performed; (B) Force curve obtained from doing force pulling at a micelle at the red circle from (A) showing very high adhesion; (C) 7.2 x 7.2 μm height image of fibrillar β-CN; (D) force curve obtained at the red circle on (C).

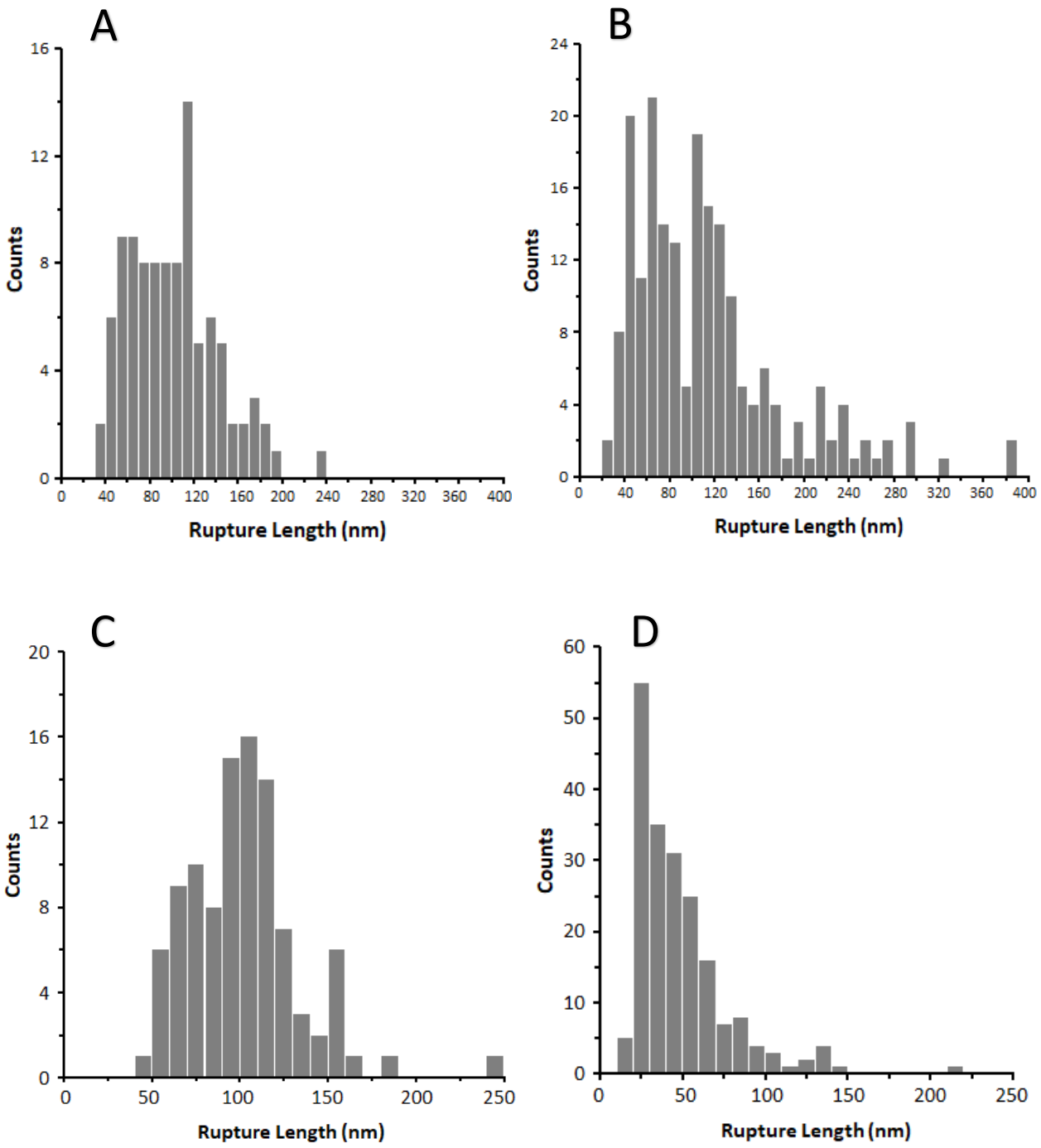

Figure 23. Histograms of rupture length for β-CN and β-LG, measured from hundreds of force curves: (A) rupture length data for native β-LG; (B) rupture length data for β-LG fibrils; (C) rupture length data for native β-CN; (D) rupture length data for β-CN fibrils.

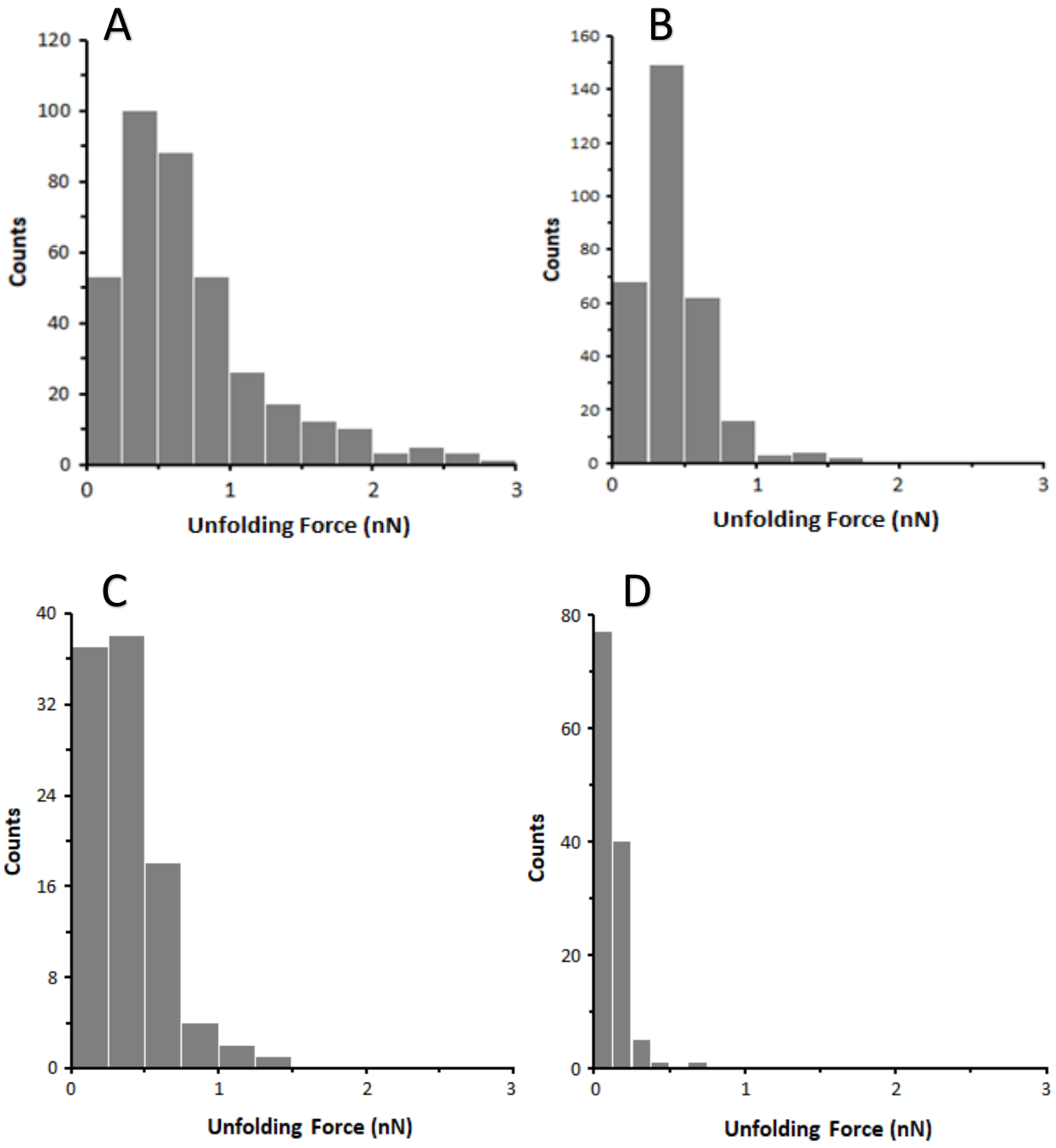

Figure 24. Histograms of unfolding force for β-LG and β-CN: (A) unfolding force data for β-LG fibrils; (B) unfolding force data for β-CN fibrils; (C) unfolding force data for native β-CN; (D) unfolding force data for native β-LG. Fibrillar β-LG has an average unfolding force almost five times greater than the native conformation and almost twice greater than that of fibrillar β-CN.

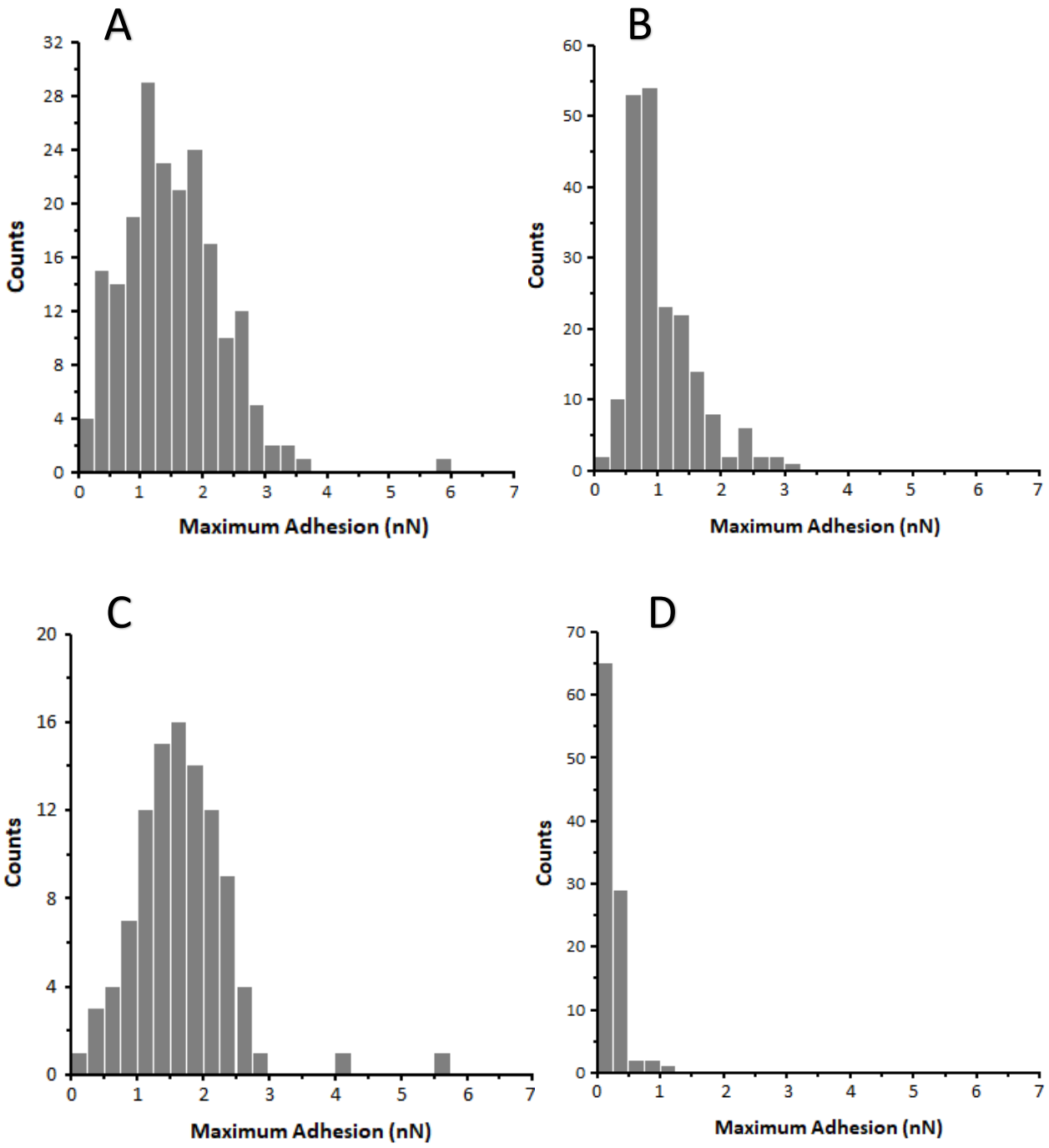

Figure 25. Histograms of maximum adhesion for β-CN and β-LG: (A) maximum adhesion data for β-LG fibrils; (B) maximum adhesion data for β-CN fibrils; (C) maximum adhesion data for native β-CN; (D) maximum adhesion data for native β-LG. Fibrillar β-LG has an average adhesion much higher than the native conformation and slightly higher than fibrillar β-CN.

4.5. Discussion

A major difficulty for this chapter was preparing a solution with a concentration (0.2 % w.t) low enough to get isolated fibrils on the mica surface, but high enough to find the fibrils quickly when imaging. After doing the image analysis, it was determined that the persistence length was 920 nm for fibrillar β-LG and 2240 nm for β-CN; the values obtained for the persistence length of β-LG are near those previously obtained by other studies; for example, two previous studies using a similar method determined Lp to be 788 nm and 1000 nm [21]. Although the persistence length is a measure of stiffness, β-CN fibrils are much thicker than those from β-LG and according to some models the Young's modulus inverse dependence on thickness more than compensates its dependence on persistence length [33]. There were three rough peaks in the rupture length histogram for the native β-LG at pH 7, the highest one corresponding to lengths of 110-120 nm, a lower one at 50- 70 nm and a much lower one at 170-180 nm; assuming that force curves show the unfolding of the globular protein and considering that β-LG has an unfolded contour length ~ 53 nm, this would agree well with previous studies showing that β-LG exists mostly as dimers in these conditions but with a good amount of monomers and a few trimers. The rupture length histogram for fibrillar β-LG showed two peaks: the highest one at 50-75 nm and another one at 100-125 nm; this peaks occur at similar lengths as those for native β-LG implying these is some structural continuity between native β-LG monomers/dimers and the β-LG nucleus which is incorporated into the fibrils (native β-LG already has a high amount of β-strands so perhaps it would only require limited denaturation before being assimilated into a fibril); Further evidence of this continuity would be the height of the thinnest β-LG fibrils ~1.5 nm, which is nearly the height that unfolded β-LG monomers adopt when adhered to a surface at pH 2 according to literature.

A possible interpretation of the force curves obtained from fibrillar β-LG would be that the AFM tip is unfolding individual fibril nuclei from the fibril surface and these are made of partially unfolded β-LG monomers and occasionally the tip would manage to peel off a second oligomer in series and this would explain the second peak in the rupture length histogram. The values for the rupture length for fibrillar β-CN do not correspond to the lengths of unfolded β-CN monomers ~ 74 nm. This could be explained by considering that β-CN monomers do not have much β-strand content in them compared to β-LG monomers; β-CN monomers would require more extreme denaturation (3 days of heating vs. 1 day for β-LG) before being incorporated into fibrils, up to the point in which the nuclei which compose the fibril are almost unrecognizable from the native β-CN conformation. Adhesion values for β-LG and β-CN fibrils were comparable and were much higher than those of the native protein in the case of β-LG but not for β-CN; β-CN has a native micelle conformation which would explain the high adhesion and shape of the force curves on Figure 22B. Because the tip is pulling at many β-CN monomers within the micelle simultaneously there will be high adhesion and the unfolding events will be irregularly spaced; however, the high adhesion persists even (but the peaks are slightly more regularly spaced) when using solutions that dissociate the protein into monomers. This could validate previous studies that argue that β-CN monomers are very deformable and form multi layers when adsorbed into a surface [19]. The average unfolding force for β-LG fibrils was 88% higher than that of β-CN fibrils; this data can be interpreted using the concept of hidden length (explained in the introduction), which argues that amyloid fibrils can withstand high stretching forces due to their folded β-strand structure (cross-β) and that this is the main reason for their high Young's modulus; a higher unfolding force corresponds to a greater hidden length or a denser packing of β-strands which in turn corresponds to a higher Young's modulus [16].

CHAPTER V

CONCLUSIONS

Self-assembled nanofibrils from milk proteins have become the subject of extensive research in recent years due to their impressive mechanical properties and their possible implementation in nanotechnology, medicine and the food industry; at the same time, the unwanted presence of amyloid fibrils in ultra-heat treated milk and other foods is considered a possible safety risk. In order to unlock the full potential of amyloid fibrils (and to prevent their formation when these are not desired) it is necessary to understand in more detail how these are formed, their structure and their mechanical properties.

In the previous two chapters we have presented the results of the application of two important AFM modes (Peakforce QNM and Force spectroscopy) to the study of amyloid fibrils formed from two relevant milk proteins (β-LG and β-CN). The results for the Young's modulus (4.3 GPa for β-LG and 3.1 GPa for β-CN) were within the range of other amyloid fibrils such as Insulin or Lysozyme and close to each other. The reasons for the similarity in mechanical properties was explained in the introduction as being due to the common cross-β structure shared by all amyloid fibrils. On chapter four the Young's modulus was found to have a possible proportionality with the average step unfolding force recorded during force spectroscopy experiments; this proportionality was again related to the cross-β structure of the fibrils and the amount of hidden length and sacrificial bonds that each fibril species contains.

Although initially the main objective of this thesis was to study the mechanical properties of the fibrils, difficulties with the preparation of the fibrils yielded some interesting information about the fibrillation process and the dependence it has on the protein concentration and heating time. β-LG required a few trials before producing the fibrils, the main difficulty was finding a high enough concentration for the fibrils to nucleate (2 % wt.) when heated for 20 hours. For β-CN the fibrillation process required five attempts until the adequate heating time was (3 full days) found. Once fibrils were produced, AFM imaging was used to measure the contour length and end-to-end distance of dozens isolated fibrils; from this data the WLC model correlation function was obtained and the persistence length of the fibrils was determined (920 nm for β-LG and 2240 nm for β-CN) and found to be in agreement with previous studies.

From the values obtained for the rupture length and the overall shape of the force curves when doing force spectroscopy experiments, we see a very close correspondence between fibrillar β-LG and native β-LG, and from this can hypothesize that the nuclei of β-LG fibrils consist of partially unfolded native monomers. For β-CN no such correspondence in rupture length data or overall force curve shape was seen between the native conformation of the protein (either β-CN that forms micelles or when it exists as monomers at very low concentrations) with the fibrillar nuclei that forms the fibrils. From this (but also taking into account our results for the heating time required for fibrillation) we argue that native β-CN requires much more extensive denaturation (and therefore longer heating time) before forming a fibril nucleus, while β-LG requires less denaturation due to its native structure already having a high percentage β-strand content when compared to native β-CN.

In conclusion, this thesis has served to extend the application of the AFM technique and two of its powerful modes to the study of a subject (amyloid fibrils from milk proteins) which has increasing relevance in biophysics. At the same time, it has served as an independent validation of previous research regarding the existence of a critical native protein concentration and a minimum heating time necessary for amyloid fibrils to form. In the case of β-LG a very close correspondence was achieved (2% wt. as minimum concentration in this thesis vs. 2.5 % for our reference). However, the aspects in which there was discrepancy when compared to previous research were the most interesting; for example, the fact that β-CN required three full days of heating at 80 ^{o}C when compared to our reference which only required 20 hours of heating at 90 ^{o}C; this opens the possibility for more detailed future research on the effect of heating time on fibrillation and whether or not there exists a critical temperature beyond which fibril formation is accelerated.

Future research involves studying heat induced fibrillation in more detail by imaging the protein at (more frequent) regular time intervals during the fibrillation process and applying the QNM and force spectroscopy modes at each step. This procedure would be repeated many times, gradually changing the preparatory conditions (such as protein concentration, temperature, pH, pressure) in order to obtain a more exact understanding of the factors at play during fibril formation and how these relate to the mechanical properties of the mature fibril. It would also be interesting to consider the relevance of the native structure of the protein to the heating time required for fibril formation; many different proteins with a wide variety of native structures should be subjected to the same denaturation inducing conditions to test whether the amount of β-strand content present in the native protein has some proportionality to the speed of fibrillation when subjected to prolonged heating at the same temperature.

AFM-QNM and AFM-force spectroscopy should be applied to study the mechanical properties and structure of co-aggregated β-LG and α-CN fibrils from an actual sample of spoiled UHT (ultra-high temperature) milk; differences in mechanical properties between β-LG/α-CN fibrils made in the laboratory and those found in milk could provide a hint of how fibrillation occurs in spoiled milk which in turn could eventually help to extend the shelf life of milk.

REFERENCES

[1] Sipe, J.D., & Cohen, A.S. (2000). Review: History of the Amyloid Fibril. *Journal of Structural Biology*, 130(2), 88-98.

[2] Mankar, S., Anoop, A., Sen, S., & Maji, S.K. (2011). Nanomaterials: amyloids reflect their brighter side. *Nano Reviews*, 2(10), 6032-6044.

[3] Ohnishi, S., & Takano, K. (2004). Amyloid fibrils from the viewpoint of protein folding. *Cellular and Molecular Life Sciences*, 61(5), 511-524.

[4] Loveday, S. M., Su, J., Rao, M. A., Anema, S. G., & Singh, H. (2012). Whey protein nanofibrils: Kinetic, rheological and morphological effects of group IA and IIA cations. *International Dairy Journal*, 26, 133-140.

[5] Oboroceanu, D. (2011). *Characterization of β-Lactoglobulin fibrillar assemblies* (Doctoral dissertation, University of Limerick, Limerick, Ireland). Retrieved from https://ulir.ul.ie/.

[6] Rambaran, R.N., & Serpell, L.C. (2008). Amyloid fibrils Abnormal protein assembly. *Prion*, 2(3), 112-117.

[7] Eisenberg, D., & Jucker, M. (2012). The Amyloid State of Proteins in Human Diseases. *Cell*, 148(6), 1188-1203.

[8] Ow, S.Y., & Dunstan, D.E. (2014). A brief overview of amyloids and Alzheimer's disease. *Protein Science*, 23(10), 1315-1331.

[9] Khurana, R., Ionescu-Zanetti, C., Pope, M., Li, J., Nielson, L., Ramírez-Alvarado, M.,… Carter, S.A. (2003). A General Model for Amyloid Fibril Assembly Based on Morphological Studies Using Atomic Force Microscopy. *Biophysical Journal*, 85(2), 1135-1144.

[10] Galzitskaya, O.V., Dovidchenko, N.V., & Selivanova, O.M. (2016). Kinetics of Amyloid Formation by Different Proteins and Peptides: Polymorphism and Sizes of Folding Nuclei of Fibrils. In A.R. Fernandez-Escamilla (Ed.), *Exploring New Findings on Amyloidosis* (pp. 145-166). London, U.K: InterchOpen.

[11] Arnaudov, L.N., de Vries, R., Ippel, H., & van Mierlo, C.P.M. (2003). Multiple Steps during the Formation of β-Lactoglobulin Fibrils. *Biomacromolecules*, 4(6), 1614-1622.

[12] Gosal, W.S., Morten, I.J., Hewitt, E.W., Smith, D.A., Thomson, N.H., & Radford, S.E. (2005). Competing Pathways Determine Fibril Morphology in the Self-assembly of β2-Microglobulin into Amyloid. *Journal of Molecular Biology,* 351, 850-864.

[13] Calamai, M., R. Khumita, J., Mifsud, J., Parrini, C., Ramazzotti, M., Ramponi, G.,… Dobson, C.M. (2006). Nature and Significance of the Interactions between Amyloid Fibrils and Biological Polyelectrolytes. *Biochemistry*, 45 (42), 12806–12815.

[14] Serpell, L. (2014). Amyloid structure. *Essays In Biochemistry*, 56, 1-10.

[15] Lamour,G., Nassar, R., Chan, P.H.W, Bozkurt, G., Li, J., Bui, J.M,…Gsponer, J.A. (2017). Mapping the Broad Structural and Mechanical Properties of Amyloid Fibrils. *Biophysical Journal,* 112(4), 584–594.

[16] Fukuma, T., Mostaert, A.S., & Jarvis, S.P. (2006). Explanation for the mechanical strength of amyloid fibrils. *Tribology Letters,* 22(3), 233-237.

[17] Schleeger, M., vanderAkker, C.C., Deckert-Gaudig, T., Deckert, V., Velikov, K.P., Koenderink, G., & Bonn, M. (2013). Amyloids: From molecular structure to mechanical properties. *Polymer,* 54(10), 2473-2488.

[18] Anna, H., Hostmark, A.T., & Harstad, O.M. (2007). Bovine milk in human nutrition – a review. *Lipids Health Dis,* 6(25), 1476-1511.

[19] Fuentes, L.P., Drummond, C., Faraudo, J. & Bastos-González, D. (2017). Adsorption of Milk Proteins (β-Casein and β-Lactoglobulin) and BSA onto Hydrophobic Surfaces. *Materials,* 10(8), 893.

[20] UniProt. Retrieved from https://www.uniprot.org/.

[21] Casein Beta (CSN2). Retrieved from http://www.cloud-clone.com/items/J332.html

[22] Berry, G.P., & Creamer, L.K. (1975). The association of bovine beta-casein. The importance of the C-terminal region. *Biochemistry*, 14(16), 3542-3545.

[23] Binnig, G., & Quate, C.F. (1986). Atomic Force Microscope. *Physical Review Letters*, 56(9), 930-933.

[24] Ccem.mcmaster.ca. (2017). *Atomic Force Microscope – Canadian Centre for Electron Microscopy*. [online] Available at: https://ccem.mcmaster.ca/atomic-force-microscope/ [Accessed 16 Oct. 2018].

[25] Hua, Y. (2014). *PeakForce-QNM* [PDF document]. Retrieved from http://mmrc.caltech.edu/AFM%20Dimension%20Icon/Bruker%20Training/Peak%20Force%20QNM_Adv%20Apps%20Training%202014.pdf.

[26] JPK Instruments. *A practical guide to AFM force spectroscopy and data analysis*. Retrieved from https://www.jpk.com/app-technotes-img/AFM/pdf/jpk-tech-force-spectroscopy.14-2.pdf.

[27] JPK Instruments. *Structural investigation of single biomolecules*. Retrieved from https://www.jpk.com/app-technotes-img/AFM/pdf/jpk-app-molecular-stretching.14-2.pdf.

[28] Bois, J. (2002). *Rudiments of Polymer Physics* [PDF document]. Retrieved from http://pimprenelle.lps.ens.fr/biolps/sites/default/files/teaching/4/poly_elast.pdf.

[29] Force Spectroscopy and Other AFM Force Measurements. Retrieved from https://afm.oxinst.com/application-detail/afm-force-measurements.

[30] Trachtenberg, S., & Hammel, I. (2010). Determining the persistence length of biopolymers and rod-like macromolecular assemblies from electron microscope images and deriving some of their mechanical properties. *Microscopy: Science, Technology, Applications and Education,* 1690-1695.

[31] Taniguchi, Y., Kobayashi, A., & Kawakami, M. (2012). Mechanical unfolding studies of protein molecules. *Biophysics (Nagoya-shi),* 8, 51-58.

BIOGRAPHICAL SKETCH

Hugo Villar Castellanos completed his Master of Science in Physics with the University of Texas Rio Grande Valley on the Fall 2018 semester. He obtained his Bachelor of Science degree in Physics from the University of Texas at Brownsville in 2015, where he worked on campus as a math and physics tutor on the Learning Enrichment Center for two semesters. He is interested in the applied areas of physics and engineering such as Biophysics and Geophysics. Personal email is hugoadrian83@hotmail.com